Title
Impacts of cloud superparameterization on projected daily rainfall intensity climate changes in multiple versions of the Community Earth System Model

Journal
Journal of Advances in Modeling Earth Systems, 8(4)

ISSN
1942-2466

Authors
Kooperman, Gabriel J
Pritchard, Michael S
Burt, Melissa A
et al.

Publication Date
2016-12-01

DOI
10.1002/2016ms000715

Peer reviewed

AGU PUBLICATIONS

Journal of Advances in Modeling Earth Systems

RESEARCH ARTICLE
10.1002/2016MS000715

Key Points:
- Superparameterization intensifies future rainfall distributions smoothly across all rain rates without sensitivity to horizontal resolution
- Future moderate and extreme rain rates intensify in regions associated with key modes of tropical variability with superparameterization
- Conventional convective parameterization does not predict intensification of moderate rain rates in tropical action centers

Supporting Information:
- Supporting Information S1

Correspondence to:
G. J. Kooperman,
gkooperm@uci.edu

Citation:
Kooperman, G. J., M. S. Pritchard, M. A. Burt, M. D. Branson, and D. A. Randall (2016), Impacts of cloud superparameterization on projected daily rainfall intensity climate changes in multiple versions of the Community Earth System Model, *J. Adv. Model. Earth Syst.*, *8*, 1727–1750, doi:10.1002/2016MS000715.

Received 12 MAY 2016
Accepted 21 SEP 2016
Accepted article online 26 SEP 2016
Published online 28 OCT 2016

Impacts of cloud superparameterization on projected daily rainfall intensity climate changes in multiple versions of the Community Earth System Model

Gabriel J. Kooperman[1], Michael S. Pritchard[1], Melissa A. Burt[2], Mark D. Branson[2], and David A. Randall[2]

[1]Department of Earth System Science, University of California, Irvine, California, USA, [2]Department of Atmospheric Science, Colorado State University, Fort Collins, Colorado, USA

Abstract Changes in the character of rainfall are assessed using a holistic set of statistics based on rainfall frequency and amount distributions in climate change experiments with three conventional and superparameterized versions of the Community Atmosphere Model (CAM and SPCAM). Previous work has shown that high-order statistics of present-day rainfall intensity are significantly improved with superparameterization, especially in regions of tropical convection. Globally, the two modeling approaches project a similar future increase in mean rainfall, especially across the Inter-Tropical Convergence Zone (ITCZ) and at high latitudes, but over land, SPCAM predicts a smaller mean change than CAM. Changes in high-order statistics are similar at high latitudes in the two models but diverge at lower latitudes. In the tropics, SPCAM projects a large intensification of moderate and extreme rain rates in regions of organized convection associated with the Madden Julian Oscillation, ITCZ, monsoons, and tropical waves. In contrast, this signal is missing in all versions of CAM, which are found to be prone to predicting increases in the amount but not intensity of moderate rates. Predictions from SPCAM exhibit a scale-insensitive behavior with little dependence on horizontal resolution for extreme rates, while lower resolution (~2°) versions of CAM are not able to capture the response simulated with higher resolution (~1°). Moderate rain rates analyzed by the "amount mode" and "amount median" are found to be especially telling as a diagnostic for evaluating climate model performance and tracing future changes in rainfall statistics to tropical wave modes in SPCAM.

1. Introduction

Anthropogenic climate change is expected to impact the character of precipitation in many ways including the total amount, frequency, and intensity of rainfall. On global scales, there are energetic constraints that provide a useful framework to assess these changes: increases in atmospheric radiative cooling require atmospheric latent heating, i.e., total accumulated surface precipitation, to increase by approximately 1–3% $°C^{-1}$ [*Allen and Ingram*, 2002; *Pendergrass and Hartmann*, 2014a; *Stephens and Ellis*, 2008] and the Clausius-Clapeyron relation suggests that rising air parcels should contain on average ~7% $°C^{-1}$ more moisture, setting a lower bound for increases in extreme rainfall if dynamics were to remain unchanged [*Allan and Soden*, 2008; *Pendergrass and Hartmann*, 2014b]. In general, the first constraint is reasonably well represented by current global climate models (GCMs) contributing to the Coupled Model Intercomparison Project Phase 5 (CMIP5) [*Pendergrass and Hartmann*, 2014a] and to some extent these models capture percentage changes in extreme rainfall that are close to the Clausius-Clapeyron value when taken as a multimodel global mean [*Pendergrass and Hartmann*, 2014c].

However, rainfall intensity changes are much less certain on an individual model level and on regional scales, where the expected response may exceed global Clausius-Clapeyron moisture scaling. Regional intensity changes depend on large-scale circulation, moisture transport, and local surface sensible and latent heat fluxes [*Seneviratne et al.*, 2010; *Trenberth*, 2011], which vary widely across models (e.g., large uncertainty is found by *Martins et al.* [2015] and *Yin et al.* [2013] for the Amazon region and *Thibeault and Seth* [2014] for the eastern United States). Observationally constrained estimates suggest that extreme rainfall (99.9th percentile rates) should increase by ~10% $°C^{-1}$ in the tropics and only ~5% $°C^{-1}$ at higher latitudes [*O'Gorman*, 2012; *O'Gorman*, 2015], but current GCMs are not able to capture these regional variations

[*O'Gorman*, 2012]. Individual CMIP3/5 GCMs predict changes that range from ~2 to 30% $°C^{-1}$ for the highest percentiles, with the largest model spread in the tropics [*O'Gorman*, 2012; *Pendergrass and Hartmann*, 2014c].

Improving our understanding and ability to predict regional changes is of critical importance for society, for both human water management and natural ecosystems. The frequency of rainfall events largely determines the prevalence of drought conditions, and the intensity of events can influence surface water runoff and flooding, both of which have important implications for freshwater storage and availability. However, confidence in projecting changes in rainfall is limited by an inability of current models to simulate the present-day representation of these high-order statistical characteristics of rainfall compared to observations. In general, conventional GCMs tend to produce weak intensity rainfall too frequently compared to observations, especially over land [*Sun et al*., 2006; *Allan and Soden*, 2008]. Making progress on this problem has been challenging because the physics that drive rainfall production depend on convective processes that can only be resolved at kilometer scales (less than 4 km), and current operational resolution for most GCMs participating in CMIP5 is on the order of 100 km. At these scales, as with the upcoming CMIP6 (~25 km), convection is represented by idealized parameterizations [e.g., *Arakawa and Schubert*, 1974; *Zhang and McFarlane*, 1995], which diagnostically estimate convective precipitation from large-scale instabilities rather than explicit prognostic calculation. This requires assumptions about spatiotemporal scales (i.e., horizontal resolution [*Kopparla et al*., 2013] and convective adjustment time scales [*Gustafson et al*., 2014]) that are poorly known and may vary with region or type of convection.

In this study, we evaluate changes in daily rainfall as simulated by a GCM that avoids these assumptions and explicitly permits convective-scale processes in a framework that remains coupled to large-scale circulation and global energetics. The approach is called cloud superparameterization (SP), which embeds simplified cloud-resolving models in each column of a conventional GCM to resolve convection and clouds on kilometer scales, and replace statistical convective and boundary layer parameterizations [*Randall et al*., 2003]. The analysis here focuses on the implementation of this method in several versions of the Community Atmosphere Model (CAM and SPCAM), described in detail below, and builds on an assessment of present-day/preindustrial rainfall using identical model versions published in *Kooperman et al*. [2016].

Kooperman et al. [2016] demonstrated that superparameterization improves the intensity of both moderate and extreme rain rates relative to Tropical Rainfall Measuring Mission (TRMM) 3B42 version 7 rainfall observations, especially in tropical regions associated with the Madden Julian Oscillation (MJO) and monsoons. In particular, *Kooperman et al*. [2016] identified that moderate rainfall rates, which contribute the most accumulated surface rainfall (i.e., peak in the rainfall amount distribution—*rainfall amount mode*), are better represented in SPCAM, without sensitivity to horizontal resolution. In contrast, CAM and SPCAM have similar intensity statistics at high latitudes, where much of the rainfall is produced by resolved-scale process in CAM, and also show similar mean rainfall and dry day frequency biases. Previous work has shown general improvements in tropical convection with SPCAM, which captures the convective variability associated with the MJO [*Benedict and Randall*, 2009], monsoons [*DeMott et al*., 2011; *Stan and Xu*, 2014], and tropical waves [*Khairoutdinov et al*., 2005; *McCrary et al*., 2014]. Simulated organized convective systems in the midlatitudes during summer have also been shown in SPCAM, particularly in the central United States [*Pritchard et al*., 2011; *Kooperman et al*., 2013]. These improvements in convection contribute to more realistic rainfall intensity shown by *Kooperman et al*. [2016] on global scales, and previously on regional scales for rainfall timing and intensity [*DeMott et al*., 2007; *Li et al*., 2012; *Pritchard and Somerville*, 2009a, 2009b; *Rosa and Collins*, 2013].

SPCAM predictions of future rainfall changes have also been evaluated in several studies. On global scales, mean rainfall was assessed by *Stan and Xu* [2014], who found that SPCAM simulates a similar mean pattern of precipitation change as CAM, with the largest increases in rainfall over the equatorial Pacific, Indian Ocean, and Maritime Continent, and reductions in rainfall over tropical South and central America and most subtropical regions. Regionally, along the eastern United States, *Zhu and Stan* [2015] found an opposite response in SPCAM relative to CAM—a decrease in precipitation during summer driven by differences in large-scale modes over the Atlantic Ocean and a local soil moisture reduction. Over the central United States, *Kooperman et al*. [2014] assessed rainfall intensity changes associated with mesoscale convective systems and found a significant increase in the intensity of rainfall from organized summer storms in SPCAM. Additionally, recent investigation of the response of the MJO to climate forcing demonstrates a

significant amplification (e.g., stronger, faster, and more frequent) with higher CO_2 concentrations [*Arnold et al*., 2014] as well as enlargement over warmer sea-surface temperatures [*Pritchard and Yang*, 2016]. Since the MJO and monsoonal systems modulate rainfall intensity in the present climate [*Kooperman et al*., 2016], changes in these convection systems are also expected to modulate future changes in rainfall intensity.

Here we investigate changes in rainfall, focusing particularly on frequency and intensity on global scales for the first time, using a set of diagnostics based on precipitation frequency and amount distributions [*Kooperman et al*., 2016; *Pendergrass and Hartmann*, 2014b]. These diagnostics are described in detail in section 2 below, along with descriptions of the models and simulation design. An overview and general discussion of the results is given in section 3, and the major findings and conclusions are summarized in section 4.

2. Background

A brief description of the methods, models, and simulations is given here; for more details, see *Kooperman et al*. [2016], which presented the present-day/preindustrial analysis methodology on which this climate change analysis is rooted.

2.1. Methods—Rainfall Distributions

Changes in rainfall characteristics in response to climate forcing are evaluated using several statistics of the daily rainfall frequency and amount distributions. The distributions were created from histograms with discrete logarithmically spaced rain rate bins following *Pendergrass and Hartmann* [2014b]. With logarithmic bin spacing, the bin widths increase with higher rain rates, efficiently sampling rates from drizzle to extremes, and are related to their bin central value by a fixed percentage—10% in this study (i.e., $\Delta R/R = 0.1$, where R is rain rate bin centers and ΔR is the bin widths). We apply a dry day threshold of 0.1 mm d^{-1} (the threshold used in *Chou et al*. [2012] and *Sun et al*. [2007]), such that the first bin has an approximate width of 0.01 mm d^{-1}, and there are roughly 100 bins that span rates from 0.1 to 1000 mm d^{-1}. Applying this bin structure, the frequency distribution, amount distribution (i.e., amount of accumulated rainfall contributed by each rain rate bin), and rain rate percentile distribution is calculated using area weighted averaging over each region of interest. For a full mathematical formulation and detailed description of this method, see *Kooperman et al*. [2016] or *Pendergrass and Hartmann* [2014b].

As demonstrated in *Kooperman et al*. [2016] and *Pendergrass and Hartmann* [2014b], evaluating statistics of these rainfall distributions is a powerful way to assess the representation of simulated rainfall intensity compared to present-day observations across vast geographic areas. An example of the present-day frequency, amount, and percentile distributions is shown in the black line in Figures 1a–1c, which is depicted on a logarithmic rain rate *x* axis for Figures 1a and 1b, and a logarithmic reduction percentile *x* axis for Figure 1c, respectively, to be consistent with the logarithmic bin structure and emphasize the right tail of the distribution. These plots are useful for visualizing key characteristics of simulated rainfall including: rainy/dry day frequency (right and left of the green dry day threshold line in Figure 1a, respectively), mean rainfall (light grey area under the black line in Figure 1b), rainfall amount mode (i.e., the rate that generates the most accumulated rainfall; dark grey line in Figure 1b), and 99th percentile rate (light blue line in Figure 1c).

These distributions can also be a powerful tool for investigating the rainfall intensity response to climate change. *Pendergrass and Hartmann* [2014c] developed a framework for assessing this as a function of the initial distribution by decomposing the response into two modes, one mode with a fixed percentage increase in the amount of rain from all rates and another mode capturing a shift in the intensity without increases to the total amount of rain. This framework was expanded in *Pendergrass and Gerber* [2016] to describe changes to the rainfall distribution and their connection to the skewness of the vertical velocity distribution, which suggests additional modes may also be important. Following this approach, the magnitude of these idealized modes must be fit to simulated changes, since there is no theory to describe changes in the intensity of the entire distribution. Increases in low-level moisture [*Allan and Soden*, 2008] or changes in the moist-adiabatic lapse rate [*O'Gorman and Schneider*, 2009] may provide lower bounds on extreme rain rate changes, but these could be satisfied by either a shift in the entire distribution or an increase in the relative amount of rain from only the heaviest rates. The latter implies a change in shape, which may be difficult to fit to an initial distribution or connect to a theoretical value.

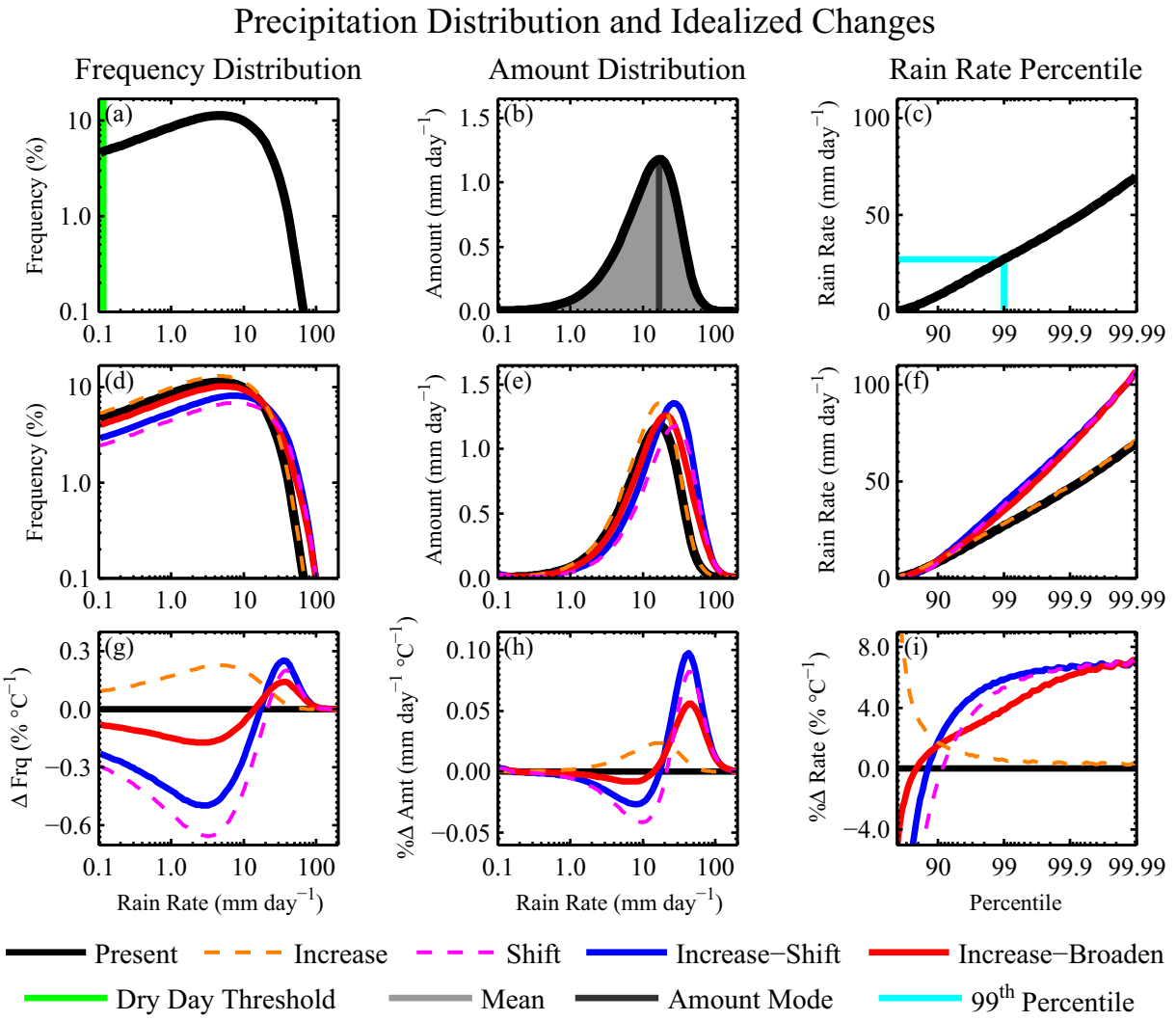

Figure 1. Precipitation (a, d, g) frequency distribution (%), (b, e, h) amount distribution (mm d^{-1}), and (c, f, i) percentile precipitation rates (mm d^{-1}) from global annual present-day GPCP 1DD daily precipitation with idealized amount increases (2% °C^{-1}) and extreme intensity shifts (7% °C^{-1}) for (a–f) distributions, (g, h) distribution change per degree, and (i) distribution percent change per degree. Note that the (a) frequency distribution is shown on a logarithmic *y* axis to capture the right tail of the distribution, but the (d) frequency distribution change is shown on a linear *y* axis. See section 2.1 for more details.

Here instead of fitting climate changes of the rainfall distribution to predefined modes, we explicitly evaluate changes to specific characteristics of the distribution. Nonetheless, before proceeding, it is useful to review several idealized climate change modes, which provide a conceptual framework for understanding key figures in our analysis, and help illustrate how potential changes to the distribution could satisfy theoretical physical constraints. As illustrated previously in *Pendergrass and Hartmann* [2014c], the change in rainfall distributions associated with an increase (e.g., 2% °C^{-1} total rainfall amount—orange dashed line), a shift (e.g., 7% °C^{-1} for the most extreme percentiles—purple dashed line), and an increase plus shift together (*increase-shift*—blue line) are shown in Figure 1. An alternative response that will prove relevant to CAM's rainfall change is also depicted in the red line (*increase-broaden*), in which half of the distribution captures the necessary increase in total rainfall and half of the distribution captures the necessary shift in intensity separately. This response effectively broadens the distribution, increasing the amount of rain on the right tail without significantly shifting the location of the peak (i.e., amount mode). The full distributions for these idealized changes are shown in Figures 1d–1f, while the differences relative to the initial distribution (black line) are shown in Figures 1g–1i, with absolute changes per degree for Figures 1g and 1h and relative percent changes per degree in Figure 1i.

A general overview of four important distribution characteristics analyzed here (mean rainfall, dry day frequency, extreme rainfall intensity, and rainfall amount mode) is provided in *Kooperman et al.* [2016], which also describes their calculation in detail. Here a brief description relevant to changes in the distributions is given based on the idealized responses depicted in Figure 1.

Mean rainfall changes are depicted in Figure 1h as differences in the integral area above and below zero in units of mm d^{-1} $°C^{-1}$. The mean can be calculated independently, but visualizing its connection to the distribution helps discriminate which rain rates contribute most. For example, an intensity shift (purple dashed line) has no overall mean change; the original distribution (black line) is simply shifted in Figure 1e. However, Figure 1h shows that there is an equal reduction in the total accumulated rain from light ($\sim$1–10 mm d^{-1}) to moderate ($\sim$10–30 mm d^{-1}) rates and increase from heavy rates (greater than 30 mm d^{-1}). The amount increase-only (orange dashed line), increase-shift (blue line), and increase-broaden (red line) have the same overall change in accumulated rain, but when a shift is included the change is produced by a narrower range of rates on the right side of the distribution. Also, broadening (red line) produces a smaller reduction in light rain relative to an intensity shift of the entire distribution (blue line). Changes in mean rainfall are discussed in section 3.2 below.

Dry day frequency (i.e., percent of days with less than 0.1 mm of accumulated rain) changes are most evident as changes in the frequency distribution of rainy day rates shown in Figure 1g, since "dry days" are not shown on a logarithmic *x* axis. With an amount increase only (orange dashed line) the frequency increases across all rates, indicating a decrease in dry days. Although there is no change in total accumulated rainfall with the intensity shift only (purple dashed line), there is a large reduction in the frequency of rainy days (i.e., increase in dry days)—when it rains harder it does not rain as often to produce the same amount of rain. The combined amount and intensity increases (red and blue lines) produce smaller reductions in overall frequency, especially for the broadening case. Changes in dry day frequency are discussed in section 3.3 below.

Extreme rainfall intensity changes are best represented by the relative percent changes per degree as a function of rain rate percentiles, focusing especially on the highest percentiles (i.e., 90th to 99.99th), as show in Figure 1i. Increasing the amount of rain by an equal percentage across all rates (orange dashed line) produces only a small increase in the intensity of the highest percentiles, while shifting the distribution toward heavier rates (purple dashed line) captures an increase in the intensity of the highest percentiles. The combined effect of increasing the amount and intensity (red and blue lines) produces a similar amplification of the highest percentile rain rates as the shift only response, though the increase-shift (i.e., smooth increase across all rates—blue line) levels off faster than the increase-broaden (red line) response. Changes in extreme rainfall intensity, focusing on the 99th percentile, are discussed in section 3.4 below.

The *rainfall amount mode* is an important metric of moderate rainfall intensity that is represented by the peak in the amount distribution (dark grey line in Figure 1b; i.e., the rain rate associated with the most accumulated rainfall), which was highlighted in *Kooperman et al.* [2016] for its key role in the hydrological cycle. Changes in the amount mode are especially important because they indicate a change in the intensity of most rain events, not only the extreme infrequent events. It is preferable to view changes in the mode in context of the original distribution (Figure 1e) because it can be difficult to interpret the shift in the difference plots alone (Figure 1h). For example, the shapes of the intensity-only (purple dashed line), increase-shift (blue line), and increase-broaden (red line) responses in Figure 1h appear very similar, and it is unclear how much the peak of the distribution shifts. However, the baseline distributions in Figure 1e show clearly that the increase-shift response (blue line) moves the peak more than the increase-broaden response (red line).

In practice, the amount mode can be difficult to calculate at the grid point level because it depends on a fit to discrete logarithmically spaced bins, which can be undersampled in regions with infrequent rainfall. Furthermore, changes in the mode calculated based on the distribution are limited to discrete logarithmic differences, which can be noisy to visualize geographically. Therefore, a complementary metric, the *rainfall amount median* (i.e., the rain rate where half the accumulated rain comes from weaker/heavier rates), which can be calculated independently of the distribution, is preferable for visualizing the geographic pattern of moderate rainfall changes. While the mode and median do not measure the exact same feature of the distribution, they do have very similar present-day geographic patterns, as shown in *Kooperman et al.* [2016]. Changes in the amount mode and median are discussed in section 3.5 below.

Another important consideration when evaluating rainfall intensity changes is whether absolute changes (mm d^{-1} $°C^{-1}$) or percentages changes (% $°C^{-1}$) are more relevant, and there are compelling arguments for both: percentages changes are directly comparable to potential theoretical constraints (i.e., 2% $°C^{-1}$ total amount and 7% $°C^{-1}$ extreme increases) discussed above, but absolute changes are more relevant to atmospheric energetics and physical processes (i.e., canopy interception and soil infiltration rates), which impact surface runoff, flooding, and groundwater. Most importantly, percentages changes potentially mask biases in the present-day representation of intensity. If the baseline rainfall is weak, as in most GCMs, then only a small absolute increase is needed to produce a large percentage increase. Likewise, a large absolute change will yield a small percentage change if the initial distribution is already more intense.

In *Kooperman et al*. [2016], we argued that the more realistic (and intense) rainfall distributions captured with superparameterization suggest it more accurately simulates the modulation of rainfall intensity by important modes of convective variability (e.g., the MJO, monsoons, and tropical waves), and may produce more reliable climate change projections. Therefore, our analysis below focuses primarily on absolute changes that take into account the representation of present-day rain rates. This differs from previous studies that have evaluated percentage changes and have suggested GCMs that capture the expected percentage changes are reliable for climate change assessment.

2.2. Community Atmosphere Model

As in *Kooperman et al*. [2016], here we analyze three conventional and superparameterized (SP) versions of the Community Atmosphere Model (CAM), coupled within the Community Earth System Model version 1 (CESM1) and the Community Climate System Model version 4 (CCSM4). For this study, CESM1 is run with both CAM versions 4 and 5 (CAM4 and CAM5), which have important physical parameterization differences, and CCSM4 is run with CAM4, all using the finite volume dynamical core.

In the following discussion, general results relevant to all three configurations of the conventionally parameterized model are referred to by shorthand as "CAM," while individual model versions are specified as CCSM4, CESM1-CAM4, and CESM1-CAM5. Each conventionally parameterized version of CAM is also run with a corresponding superparameterized counterpart (i.e., SPCCSM4, SPCESM1-CAM4, and SPCESM1-CAM5), and results relevant to all three superparameterized versions are referred to by shorthand as "SPCAM." Robust effects of superparameterization are made clear by comparing the sets of SPCAM and CAM, while the impacts of atmospheric model versions are evident comparing (SP)CESM1-CAM4 to (SP)CESM1-CAM5 and differences due to the coupled system are evident comparing (SP)CCSM4 to (SP)CESM1-CAM4.

Brief overviews, including differences between model versions, of CAM and SPCAM are provided below. For the complete scientific descriptions of CAM4 and CAM5, see *Neale et al*. [2010a, 2010b], respectively, and for details of SPCAM, see *Khairoutdinov and Randall* [2001] and *Wang et al*. [2011]. For details of the other components of CESM1/CCSM4 (i.e., interactive land, ocean, and sea-ice), see *Lawrence et al*. [2011] for the Community Land Model version 4 (CLM4), *Smith et al*. [2010] for the Parallel Ocean Program version 2 (POP2), and *Hunke and Lipscomb* [2008] for the Community Ice CodE version 4 (CICE4). A general overview of the fully coupled system in CCSM4 and SPCCSM4 is given in *Gent et al*. [2011] and *Stan and Xu* [2014], respectively.

2.2.1. Conventional-Parameterization

Both versions of CAM4 and CAM5 represent subgrid deep convection as ensembles of convective updraft plumes that deplete convective available potential energy at a fixed time scale following the *Zhang and McFarlane* [1995] scheme, including entrainment mixing [*Raymond and Blyth*, 1992] and vertical transport of horizontal momentum [*Richter and Rasch*, 2008]. In CAM5, the representation of shallow convection is updated from the *Hack* [1994] scheme to the *Park and Bretherton* [2009] scheme, which is linked to new parameterizations of moist turbulence [*Bretherton and Park*, 2009] and cloud microphysics [*Morrison and Gettelman*, 2008]. Cloud droplets and ice activate as a function of aerosol particle number and chemical composition [*Liu et al*., 2012], and evolve in a two-moment microphysics scheme [*Morrison and Gettelman*, 2008]. The representation of radiation interactions with clouds, aerosol, and gases has also been updated from CAM4 to CAM5 with the introduction of the Rapid Radiative Transfer Model for GCMs (RRTMG) [*Neale et al*., 2010b; *Iacono et al*., 2008]. For more details on these parameterizations and other components of CAM4/5, see *Neale et al*. [2010a, 2010b].

2.2.2. Superparameterization

In SPCAM, the parameterizations of deep and shallow convection described above are replaced by array-mean convective tendencies from embedded cloud-resolving models (CRMs) that represent unresolved subgrid moist convection explicitly [*Benedict and Randall*, 2009; *Randall et al*., 2003]. Each grid-column of CAM hosts an independent CRM configured at kilometer-scale resolution in two dimensions with periodic boundaries, which resolves convective-cloud processes on their native scales, while large-scale dynamics are resolved on the outer GCM grid. Running thousands of embedded CRMs makes SPCAM roughly a 100 times more computer intensive than a conventional GCM, but their independent configuration makes SPCAM massively parallel and affordable for century-long simulations [*Pritchard and Bretherton*, 2014; *Stan and Xu*, 2014]. The main updates from CAM4 to CAM5 are also present in changes from SPCAM4 (i.e., SPCCSM4 and SPCESM1-CAM4) to SPCAM5 (i.e., SPCESM1-CAM5) [*Wang et al*., 2011], including an interactive aerosol treatment [*Gustafson et al*., 2008] that links to a two-moment cloud microphysics scheme [*Morrison et al*., 2005] and the RRTMG radiative transfer scheme. For more details on superparameterization in general, see *Khairoutdinov and Randall* [2001], and for SPCESM1-CAM5-specific details, see *Wang et al*. [2011].

2.3. Simulations and Configurations

The simulations analyzed here were originally designed for two separate experiments with different configurations, but each version of SPCAM is consistent with its CAM counterpart.

The (SP)CCSM4 simulations were run with the Representative Concentration Pathway 8.5 (RCP8.5) emissions scenario (~1370 ppm CO_2-equivalent by 2100) for the 21st century [*Taylor et al*., 2012], and configured with a GCM horizontal resolution of 0.9° × 1.25° (~1°) and 30 vertical levels. In SPCCSM4, the CRM was run with 32 columns at 3 km horizontal resolution oriented in the east-west direction. The first 10 years (2006–2015) were evaluated as present-day climate (PC) conditions and the last 10 years (2091–2100) were evaluated as future climate (FC) conditions. A general overview of the results from this experiment design is given by *Meehl et al*. [2012] for CCSM4 and *Stan and Xu* [2014] for SPCCSM4.

The CESM1-CAM4 and CESM1-CAM5 simulations were run as a 4X CO_2 experiment with three segments: (1) fixed preindustrial greenhouse gas concentrations (~285 ppm CO_2), (2) CO_2 ramp up at 1% yr^{-1} to 4X preindustrial concentration, and (3) fixed 4X preindustrial CO_2 concentration (~1140 ppm CO_2), configured with a GCM horizontal resolution of 1.9° × 2.5° (~2°) and 30 vertical levels. Ten year SPCESM1-CAM4 and SPCESM1-CAM5 simulations were branched from corresponding CAM runs for the fixed preindustrial and fixed 4X CO_2 segments, using the same GCM-scale configuration and a 32 column CRM at 4 km horizontal resolution oriented in the north-south direction. To allow the climate to adjust and soil moisture fields to spin-up after branching, only the last 5 years of each segment are analyzed. For the (SP)CESM1-CAM4 and (SP)CESM1-CAM5 set of simulations, PC is preindustrial climate and FC (future climate) is 4X CO_2 climate.

Results for each model pair (i.e., CAM and SPCAM) are shown at their original resolutions so as to retain the maximum amount of information, and are therefore evaluated with respect to each other. Though the simulation setup and resolution differs from (SP)CCSM4 to (SP)CESM1-CAM4 and (SP)CESM1-CAM5, we focus on results that are consistent across all model versions and are statistically significant in the relatively short (10 and 5 years) evaluation periods to identify robust effects of cloud superparameterization on simulated rainfall properties.

3. Results

3.1. Temperature Change

Although surface temperature changes are not the focus of this paper, they are used to normalize precipitation changes across the different simulations, and are therefore worth analyzing briefly first. Global annual mean surface temperature changes are given in Table 1 and the geographic pattern of the change is shown in Figure 2. The (SP)CCSM4 RCP8.5 simulations produce smaller global mean temperature changes than the 4X CO_2 simulations (3.4–3.8°C versus 4.9–5.6°C). For the simulations based on (SP)CAM4 physics, SPCAM produces a larger temperature change than CAM, which results from bigger model differences between present-day/preindustrial temperatures rather than future temperatures. For the simulations based on (SP)CAM5 physics, SPCAM produces a smaller temperature change than CAM, which may result from

Table 1. Global Annual Mean Surface Temperature and Surface Temperature Change (°C)

Models	Present/ Preindustrial	Future Climate	Climate Change
CCSM4	14.7	18.2	3.4
SPCCSM4	13.9	17.7	3.8
CESM1-CAM4	13.7	18.8	5.1
SPCESM1-CAM4	13.3	18.7	5.4
CESM1-CAM5	13.5	19.2	5.6
SPCESM1-CAM5	14.2	19.1	4.9

updates to a two-moment cloud microphysics scheme, the RRTMG radiation scheme, and/or a modal aerosol scheme; the relative contributions from each update cannot be separated with the current simulations. However, despite the differences in forcings and model physics, the global mean changes are fairly consistent across model versions, as are their geographic patterns of change. In all simulations, the forcing is large enough to produce statistically significant differences between the two averaging periods (FC-PC) almost everywhere, except in the North Atlantic Ocean south of Greenland due to changes in ocean circulation [*Stocker et al*., 2013; *Stouffer et al*., 2006]. Otherwise, all models simulate significant warming everywhere (greater than 3°C) with the largest changes over land and at high latitudes (greater than 12°C). The changes in precipitation discussed below are normalized by these global mean temperature changes in order to fairly compare the response across different model versions and experiments.

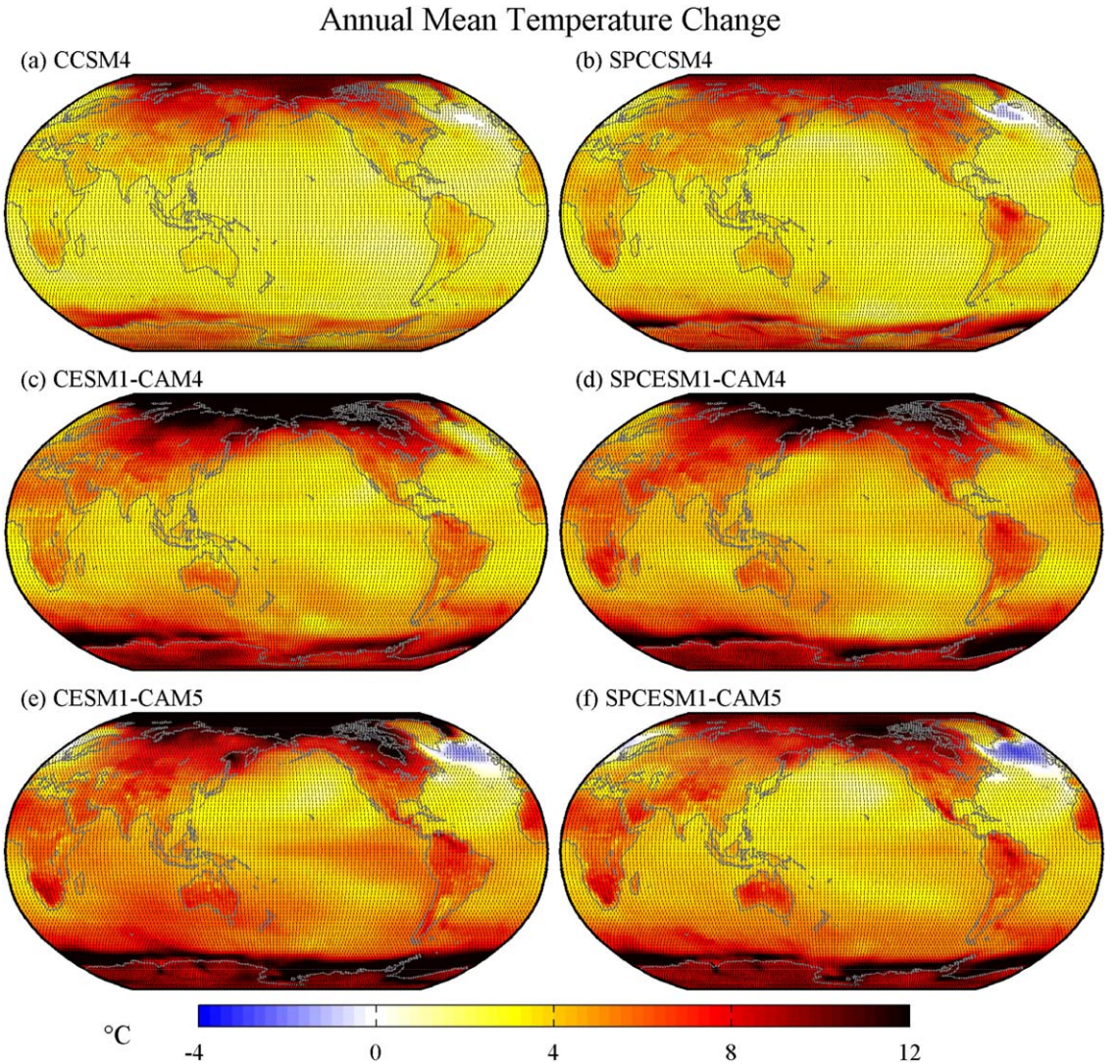

Figure 2. Annual mean temperature change (°C) from (a, b) (SP)CCSM4, (c, d) (SP)CESM1-CAM4, and (e, f) (SP)CESM1-CAM5 for (a, c, e) CAM and (b, d, f) SPCAM simulations; stippling shows significance at 95% confidence based on interannual variability; (SP)CCSM4 is shown at 1° resolution, and (SP)CESM1-CAM4 and (SP)CESM1-CAM5 are shown at 2° resolution.

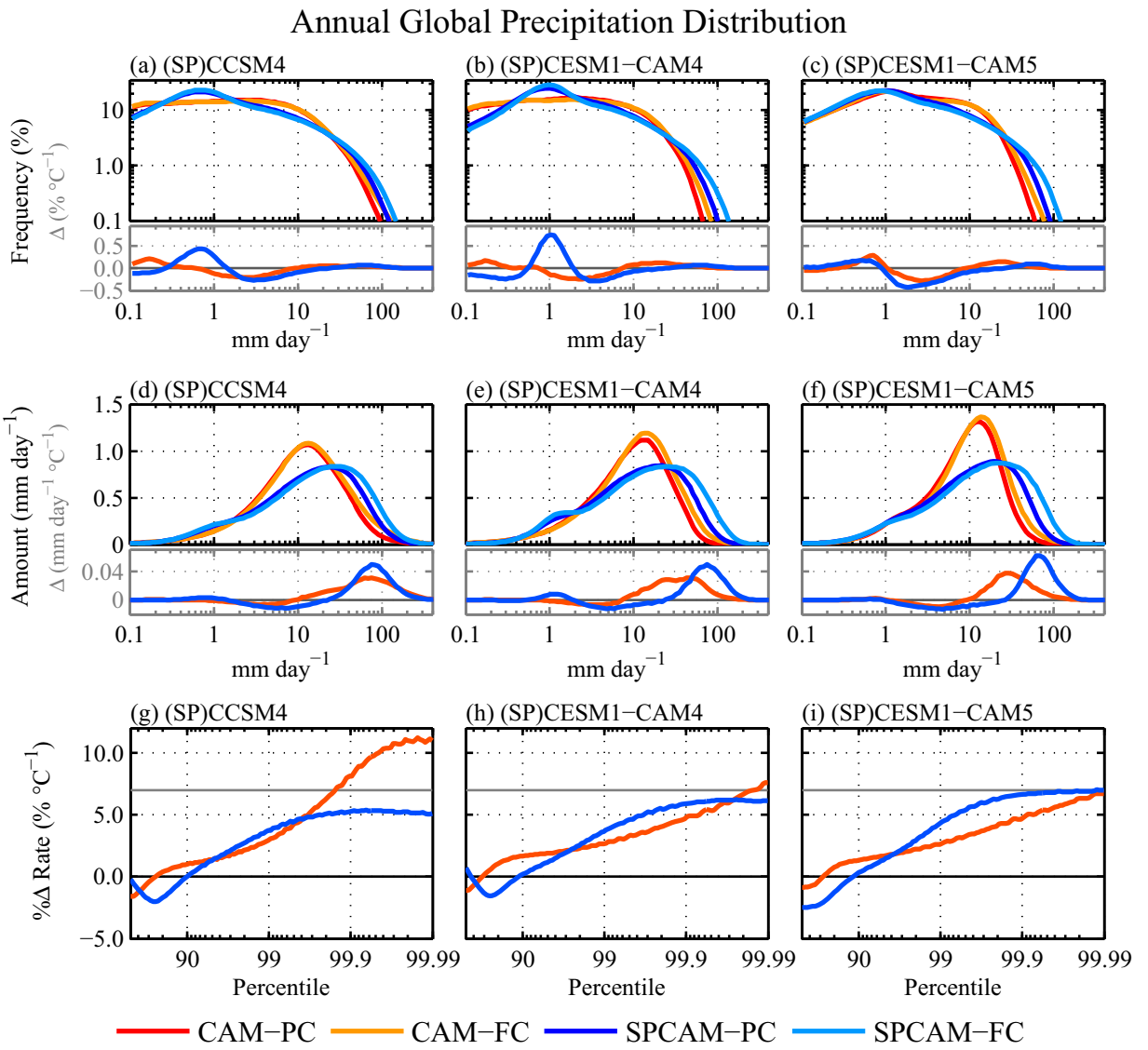

Figure 3. Precipitation (a–c) frequency distribution (%), (d–f) amount distribution (mm d^{-1}), and (g–i) percentile precipitation rate percent change per degree (% $°C^{-1}$) from global annual (a, d, g) (SP)CCSM4, (b, e, h) (SP)CESM1-CAM4, and (c, f, i) (SP)CESM1-CAM5 simulated daily precipitation; small plots show (a–c) frequency change per degree (% $°C^{-1}$) and (d–f) amount change per degree (mm d^{-1} $°C^{-1}$) for CAM (red) and SPCAM (blue); PC is present-day/preindustrial climate (red and dark blue lines); FC is future climate (orange and light blue lines); (SP)CCSM4 is shown at 1° resolution, and (SP)CESM1-CAM4 and (SP)CESM1-CAM5 are shown at 2° resolution.

3.2. Rainfall Distributions Changes

Figures 3–5 evaluate simulated changes in rainfall based on the distributions introduced in Figure 1 and described in section 2.1 above. These figures are comparable to *Kooperman et al.* [2016, Figures 2–4], which assessed the realism of present-day precipitation intensity relative to satellite observations and highlighted improvements in both moderate (∼10–30 mm d^{-1}, i.e., peak of the amount distribution—amount mode) and extreme (greater than 30 mm d^{-1}, i.e., right tail of the distributions) rainfall rates with superparameterization relative to the Tropical Rainfall Measuring Mission (TRMM) rainfall product 3B42 version 7 (TRMM 3B42). Figure 3 analyzes global rainfall distributions of frequency (top), amount (middle), and percentile rates (bottom) from CAM (red/orange) and SPCAM (light/dark blue) in versions (SP)CCSM4 (left), (SP)CESM1-CAM4 (center), and (SP)CESM1-CAM5 (right), where dark colors are present-day/preindustrial climate and light colors are future climate. The same set of distributions are also shown in Figure 4, but only for grid points with greater than 50% land fraction. Figure 5 further splits the amount distribution into five zonal average regions: two high-latitude regions (90°S–50°S and 50°N–90°N), two subtropical/midlatitude regions (50°S–15°S and 15°N–50°N), and one tropical region (15°S–15°N). Together these figures highlight

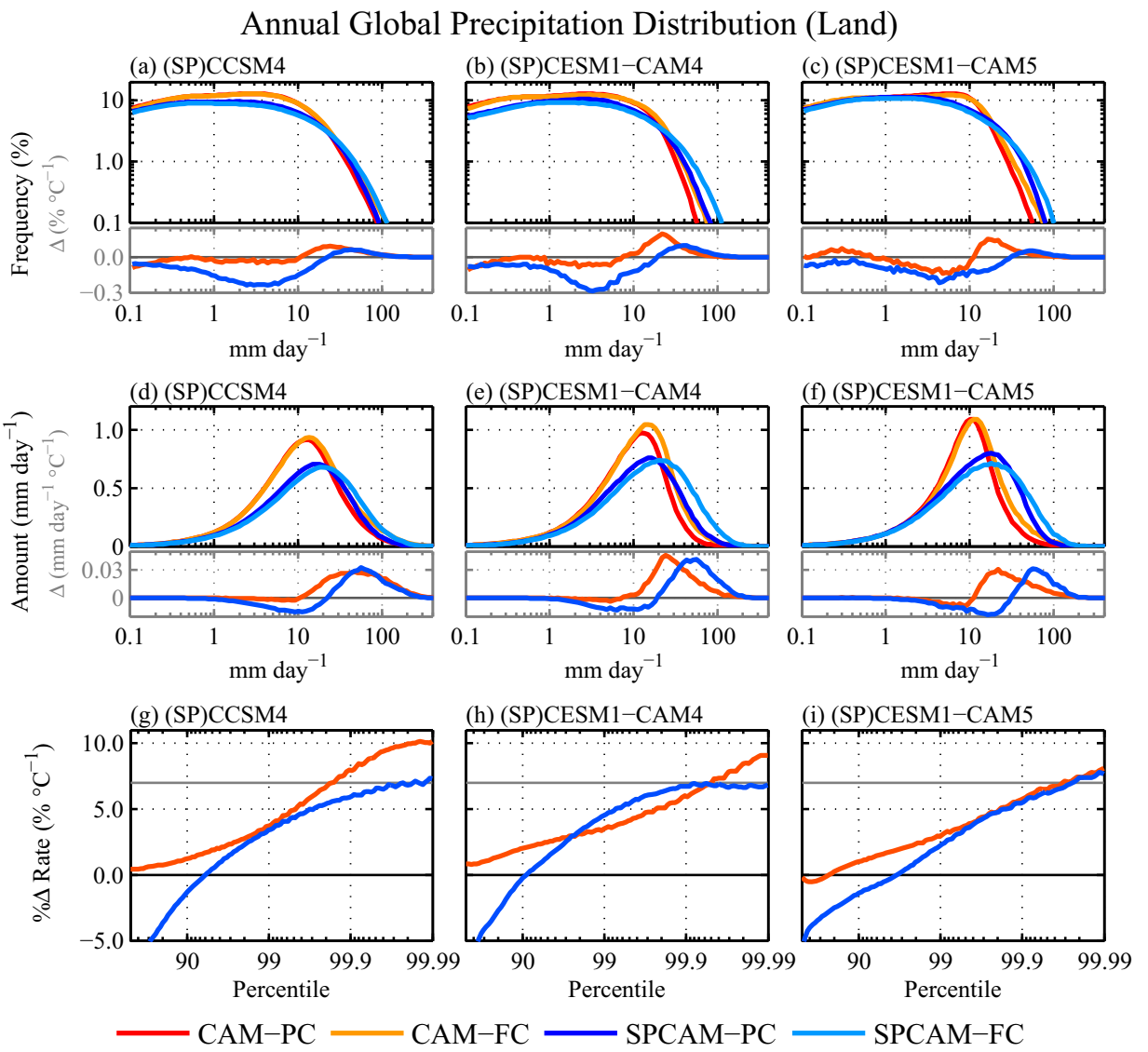

Figure 4. Precipitation (a–c) frequency distribution (%), (d–f) amount distribution (mm d^{-1}), and (g–i) percentile precipitation rate percent change per degree (% $°C^{-1}$) from global annual land-only (a, d, g) (SP)CCSM4, (b, e, h) (SP)CESM1-CAM4, and (c, f, i) (SP)CESM1-CAM5 simulated daily precipitation; small plots show (a–c) frequency change per degree (% $°C^{-1}$) and (d–f) amount change per degree (mm d^{-1} $°C^{-1}$) for CAM (red) and SPCAM (blue); PC is present-day/preindustrial climate (red and dark blue lines); FC is future climate (orange and light blue lines); (SP)CCSM4 is shown at 1° resolution, and (SP)CESM1-CAM4 and (SP)CESM1-CAM5 are shown at 2° resolution.

differences in the rainfall intensity response simulated by CAM and SPCAM, and separate the relative influence of ocean from land and tropics from middle and high latitudes.

The global frequency distributions (Figures 3a–3c, top) show a consistent response for the right tail in CAM and SPCAM, which both include more intense rates in future climates. However, the baseline intensity of the extreme tail in SPCAM is already heavier than CAM, so the future distributions reach much higher rates. In fact, the future distributions in CAM are still somewhat weaker than even the present-day/preindustrial distributions in SPCAM. These changes in extreme rainfall intensity are discussed in terms of percentile precipitation rates below (Figures 3g–3i), since their infrequency requires a logarithmic *y* axis to visualize.

An enhancement of a distinct oceanic drizzle mode (i.e., 0.8–1 mm d^{-1} peak in the frequency distribution) is seen in the baseline distributions of all versions of SPCAM and the latest version of CAM (CESM1-CAM5) [*Kooperman et al.*, 2016]. This signal tends to dominate the climate changes in the frequency distributions shown with a linear *y* axis (Figures 3a–3c, bottom), which show an increase in the versions of SPCAM based on SPCAM4 physics (SPCCSM4 and SPCESM1-CAM4). The origin of the baseline drizzle mode and its

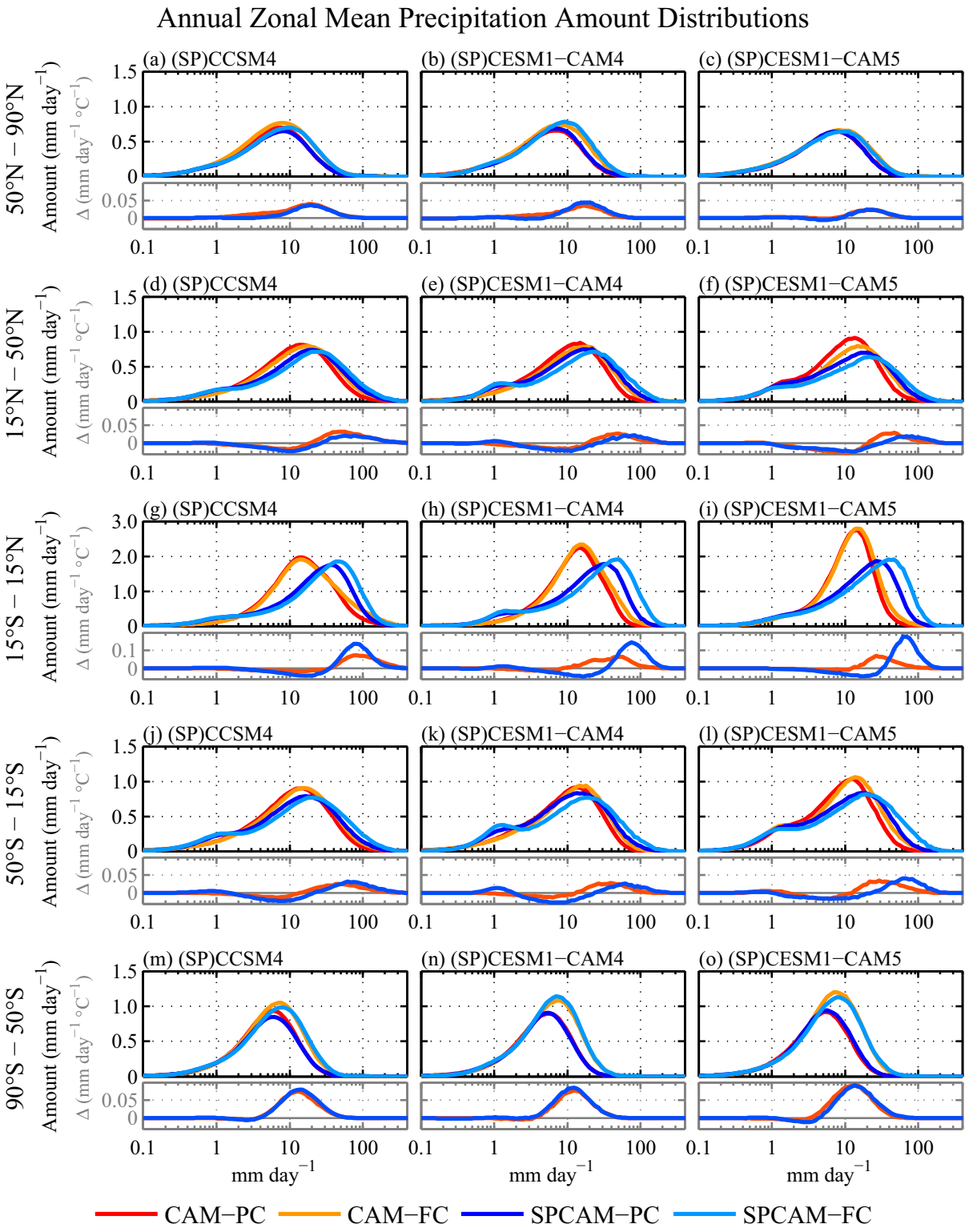

Figure 5. Precipitation amount distributions from (a–c) 50°N to 90°N, (d–f) 15°N to 50°N, (g–i) 15°S to 15°N, (j–l) 50°S to 15°S, and (m–o) 90°S to 50°S zonal averages for annual (a, d, g, j, m) (SP)CCSM4, (b, e, h, k, n) (SP)CESM1-CAM4, and (c, f, i, l, o) (SP)CESM1-CAM5 simulated daily precipitation; small plots show amount change per degree (mm d^{-1} $°C^{-1}$) for CAM (red) and SPCAM (blue); PC is present-day/preindustrial climate (red and dark blue lines); FC is future climate (orange and light blue lines); (SP)CCSM4 is shown at 1° resolution, and (SP)CESM1-CAM4 and (SP)CESM1-CAM5 are shown at 2° resolution.

enhancement with climate change is due to the representation of light rain over the ocean, since these features are not present in the land-only distributions (Figures 4a–4c, see supporting information Figure S1 for ocean-only distributions). Changes in this mode can also be seen clearly as a reduction in dry day frequency over the ocean in SPCCSM4 and SPCESM1-CAM4 (Figure 7 and section 3.4), which is not seen in corresponding versions of CAM.

Over land (Figure 4) where the drizzle mode is not present, the simulated rainfall climate change is evocative of the idealized increase-shift and increase-broaden responses (red and blue lines in Figure 1) discussed in section 2.1 above. All models simulate a reduction in the frequency of light rain (less than 10 mm d^{-1}) and an increase in heavy rain (greater than 30 mm d^{-1}). The reduction in light rain frequency is much greater in SPCAM than CAM, suggesting a larger increase-shift of the entire distribution in SPCAM, versus more of an increase-broaden of the distribution in CAM. Likewise, the location of the frequency increase is associated with more intense rain rates in SPCAM than CAM, though the magnitude of the frequency increase is larger in CAM. This relationship is expected given that movement to the right along the rainfall intensity spectrum implies a lower frequency is required to produce the same overall amount of accumulated rainfall.

Figures 3g–3i hone in on the right tail of the precipitation distribution, shown in terms of relative percentage changes per degree to be consistent with previous work [*Pendergrass and Hartmann*, 2014b, 2014c; *O'Gorman*, 2012, 2015], which are later contrasted with absolute rain rate changes assessed for the 99th percentile (section 3.5). In both CAM and SPCAM, the percentage change in intensity consistently increases with percentile from the 90th to 99.99th, but there are some interesting and suggestive differences between the two models. In SPCAM, the maximum increase levels off around the 99.5th percentile and ranges from 5 to 7% $°C^{-1}$ across all model versions with a shape similar to the idealized *increase-shift* response. In CAM, the intensity steadily increases through the 99.99th percentile, with more similarity to the idealized *increase-broaden* response and a maximum range twice as large as SPCAM from 7 to 11% $°C^{-1}$ across versions. The convex shape of the percentile distribution in CAM suggests that the extreme rates are responding independently and increasing in intensity more than the rest of the distribution.

Despite the fact that the present-day/preindustrial distributions in CAM are significantly weaker and less realistic than SPCAM, and the future changes do not shift as much in terms of absolute rain rates (see Figures 3a–3c) [*Kooperman et al*., 2016], the percentage changes are as large or larger in CAM. This is especially true for the higher (1°) resolution version of CAM in CCSM4, which has a percentage change greater than Clausius-Clapeyron. It is unknown whether this is a realistic response to changes in dynamics as well as low level moisture, which can produce super-Clausius-Clapeyron changes on regional scales [*Berg et al*., 2013], or if it represents an increase in unrealistic grid point storms that occur in some high-resolution conventionally parameterized GCMs [*Pendergrass and Hartmann*, 2014c; *Williamson*, 2013]. The maximum percentage change in the higher-resolution version of SPCAM (i.e., SPCCSM4) is more consistent with (but slightly smaller than) the lower resolution versions (i.e., SPCESM1-CAM4 and SPCESM1-CAM5), especially over land where all three versions of SPCAM reach a maximum increase of 7% $°C^{-1}$.

The consistency across resolutions and versions in SPCAM, both for the baseline percentile rates and the percentage changes, is promising evidence of the potential scale-insensitive nature of superparameterization, though it remains to be seen whether this holds for a broader range of outer-GCM and inner-CRM resolutions.

Differences in how the distributions change between the two models are perhaps clearest in the amount distributions (Figures 3d–3f). Again, all of the models increase the amount of rain from rates on the right tail of the distribution, which contributes to an increase in global mean precipitation (section 3.3). In CAM, this seems to broaden the distribution to the right, without decreasing the amount of light rain or shifting the peak ("amount mode") significantly. In general, CAM has an *increase-broaden* response (red line in Figure 1b), which appears to independently increase rain on the right shoulder. We speculate this response results from the separation of large-scale resolved processes (which produces intense rain on the right tail of the distribution) and local-scale convection (which produces the moderate rainfall peak) in CAM. In SPCAM the entire distribution appears to be part of both the amount increase and intensity responses, which shift smoothly across the distribution, with a larger reduction in light rain (less than 10 mm d^{-1}) and rightward shift in the amount mode peak.

Table 2. Annual Mean Precipitation Percent Change With 95% Confidence Interval (% °C^{-1})[a]

Region	CCSM4	SPCCSM4	CESM1-CAM4	SPCESM1-CAM4	CESM1-CAM5	SPCESM1-CAM5
90°S–90°N	1.64 ± 0.09	1.49 ± 0.17	1.65 ± 0.28	1.44 ± 0.16	1.32 ± 0.14	1.28 ± 0.17
^{L}90°S–90°N	2.31 ± 0.39	0.75 ± 0.46	2.46 ± 1.13	1.44 ± 0.93	1.51 ± 0.32	−0.02 ± 0.46
^{O}90°S–90°N	1.43 ± 0.12	1.69 ± 0.14	1.41 ± 0.16	1.43 ± 0.22	1.28 ± 0.15	1.65 ± 0.21
50°S–50°N	1.10 ± 0.14	0.93 ± 0.18	1.11 ± 0.29	0.79 ± 0.20	0.77 ± 0.18	0.77 ± 0.14
^{L}50°S–50°N	1.72 ± 0.47	−0.21 ± 0.61	1.90 ± 1.39	0.59 ± 1.21	0.92 ± 0.43	−0.88 ± 0.50
^{O}50°S–50°N	0.91 ± 0.19	1.21 ± 0.16	0.90 ± 0.21	0.84 ± 0.24	0.73 ± 0.18	1.24 ± 0.20
90°S–50°S	4.90 ± 0.35	5.70 ± 0.40	5.18 ± 0.64	6.08 ± 0.44	6.56 ± 0.45	5.83 ± 0.22
50°S–15°S	0.89 ± 0.39	0.53 ± 0.47	0.79 ± 0.38	−0.13 ± 0.57	1.31 ± 0.59	0.66 ± 0.52
15°S–15°N	1.26 ± 0.44	1.70 ± 0.29	1.69 ± 0.83	1.83 ± 0.40	1.15 ± 0.57	1.74 ± 0.51
15°N–50°N	0.97 ± 0.41	−0.18 ± 0.51	0.20 ± 0.55	−0.32 ± 0.55	−0.70 ± 0.55	−1.23 ± 0.15
50°N–90°N	4.23 ± 0.81	3.38 ± 0.43	3.74 ± 0.15	3.75 ± 0.51	2.11 ± 0.68	1.66 ± 0.88

[a]Superscripts L and O denote land-only and ocean-only averaging regions, respectively.

For rates that increase, the additional rainfall is almost the same in both models (i.e., positive area in the bottom plots of Figures 3d–3f), but the larger reduction in the amount of rain from light rates (i.e., negative area) in SPCAM contributes to a slightly smaller overall mean change relative to corresponding versions of CAM (1.64, 1.65, and 1.32% °C^{-1} for CAM and 1.49, 1.44, and 1.28% °C^{-1} for SPCAM from versions (SP)CCSM4, (SP)CESM1-CAM4, and (SP)CESM1-CAM5, respectively; Table 2). This reduction in accumulated rainfall from light rates is especially prevalent over land in SPCAM (Figures 4d–4f), where it significantly offsets the amount increase from heavier rates. The offset does not occur in CAM, which leads to a much larger increase in mean rainfall over land globally (2.31, 2.46, and 1.51% °C^{-1} for CAM and 0.75, 1.44, and −0.02% °C^{-1} for SPCAM from versions (SP)CCSM4, (SP)CESM1-CAM4, and (SP)CESM1-CAM5, respectively; Table 2). However, the regional structure leading to these global mean changes is complicated and includes areas of compensating increases and decreases, as will be seen in Figure 6.

To unfold this regional structure, the global amount distributions (Figures 3d–3f) are separated into five zonally averaged regions in Figure 5, where the two high-latitude regions (90°S–50°S and 50°N–90°N) together and the other three regions (50°S–15°S, 15°S–15°N, and 15°N–50°N) each comprise about 25% of Earth's surface area. Note that for the tropical region (Figures 5g–5i), the *y* axis range is twice that of the other regions for both the top and bottom plots, as most rainfall occurs in the tropics. From this perspective, it is clear that the differences between the two models are most pronounced in the tropics, and the results of superparameterized simulations converge with conventionally parameterized simulations with increasing latitude.

The high-latitude response is almost identical in CAM and SPCAM across all versions, where both models simulate a large amount increase and intensity shift, especially in the Southern Hemisphere. In the region from 90°S to 50°S (Figures 5m–5o), there is a clear shift in the location of the amount mode peak (∼6–9% °C^{-1}; Table 5) and a significant increase in total rainfall (∼5–6% °C^{-1}; Table 2) in both models. The high-latitude Northern Hemisphere response is smaller, but with the same general features. The fact that CAM and SPCAM produce such similar results at high latitudes, both for the baseline distributions [see *Kooperman et al.*, 2016] and the response to climate forcing, is likely due to an increased contribution from resolved-scale process in CAM with increasing latitude, where convective parameterization plays a smaller role. This suggests that superparameterization may not be necessary poleward of 50° for investigating precipitation climate changes, which could significantly reduce the computational demand of SPCAM if a regionalized load-balancer for CAM could be invented.

Transitioning through the middle and lower latitudes (15°–50°) to the tropics (15°S–15°N), the two models begin to diverge, for both the present-day/preindustrial distributions and climate change response. Differences in the tropical response contain the dominant features of the global distribution changes analyzed earlier in Figure 3. In the tropics, SPCAM's baseline distributions are much more intense than CAM's and capture the intensity observed by the TRMM 3B42 data set [*Kooperman et al.*, 2016]. The tropical rainfall response in SPCAM includes a large shift toward heavier rain rates, with more accumulated rain from the right tail of the distribution, and a reduction in the amount of rain from light and moderate rates. CAM has a smaller increase in the amount of rain from heavy tropical rates, with very little reduction in lighter rain. Again, CAM seems to increase the right shoulder of the distribution without shifting the location of the

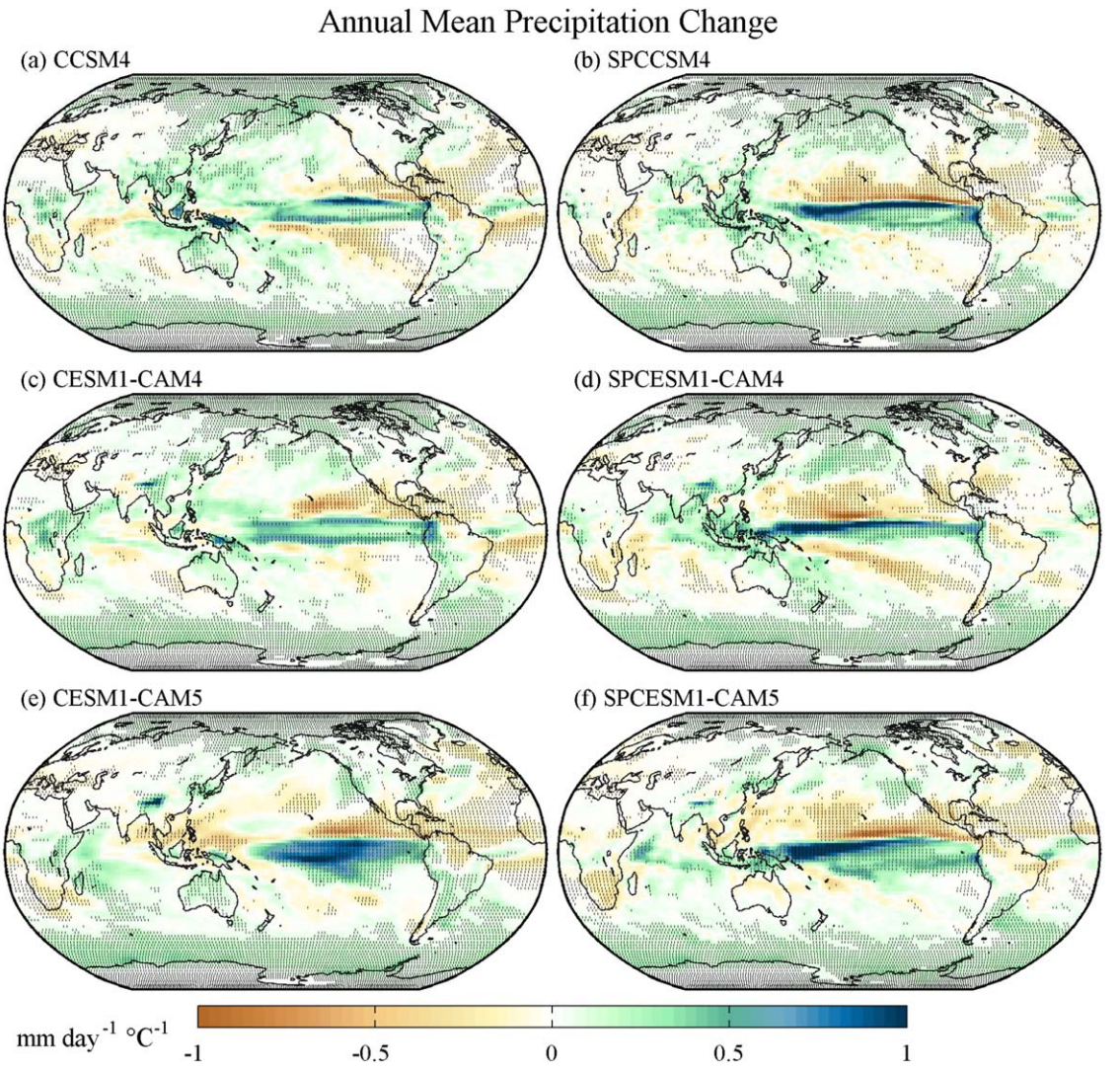

Figure 6. Annual mean precipitation change per degree (mm day^{-1} °C^{-1}) from (a, b) (SP)CCSM4, (c, d) (SP)CESM1-CAM4, and (e, f) (SP)CESM1-CAM5 for (a, c, e) CAM and (b, d, f) SPCAM simulations; stippling shows significance at 95% confidence based on interannual variability; (SP)CCSM4 is shown at 1° resolution, and (SP)CESM1-CAM4 and (SP)CESM1-CAM5 are shown at 2° resolution.

peak. The smaller increase on the right side and smaller decrease on the left side of the distribution in CAM contribute to producing a similar mean response (1.2–1.8% °C^{-1}; Table 2) across the tropics in both models.

Honing in on two metrics (amount mode and 99th percentile rates) of the intensity response highlights differences in the behavior of moderate and extreme rainfall. Although the extreme tail reaches higher rates in SPCAM, percentage changes in the 99th percentile rates are similar between the two models in the tropics, especially for the high-resolution (1°) version (SP)CCSM4 (4.93 and 4.87% °C^{-1} for CAM and SPCAM, respectively). The 99th percentile responses in the 2° CAM simulations are weaker than their SPCAM counterparts (3.88 and 3.22% °C^{-1} for CAM and 5.36 and 5.98% °C^{-1} for SPCAM from versions (SP)CESM1-CAM4 and (SP)CESM1-CAM5, respectively; Table 4), indicating some resolution dependence for extremes in conventionally parameterized versions of CAM, as has been shown previously [*O'Brien et al*., 2016; *Yang et al*., 2014].

The most significant bifurcations in the models' climate change predictions occur for *moderate* rainfall rates in the tropics. The intensity of the amount mode peak has a large shift in SPCAM, but little or no shift in CAM (0.00, 0.00, and 1.78% °C^{-1} for CAM and 8.68, 8.65, and 9.40% °C^{-1} for SPCAM from versions (SP)CCSM4, (SP)CESM1-CAM4, and (SP)CESM1-CAM5, respectively; Table 5). SPCAM's predictions indicate

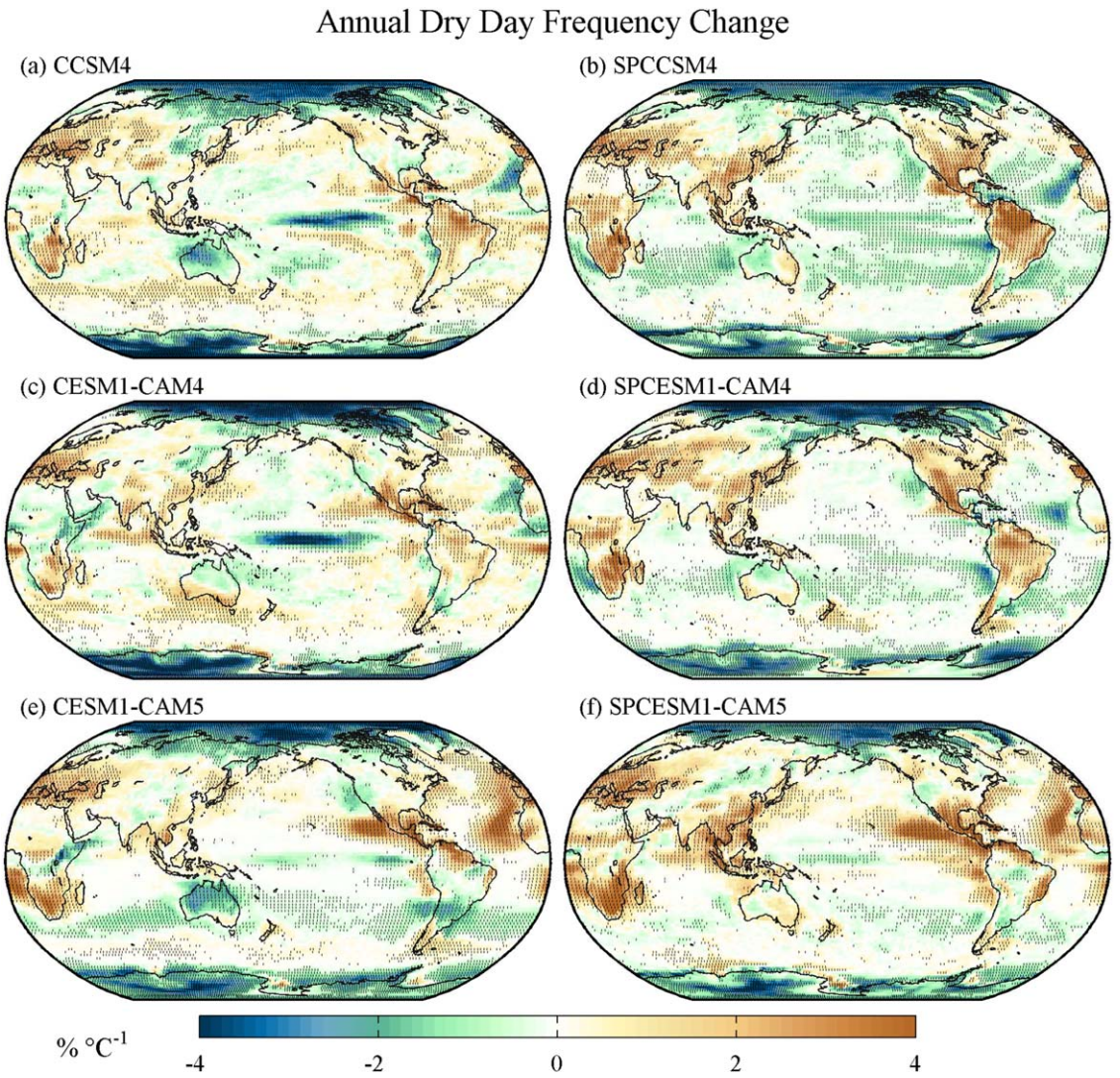

Figure 7. Annual dry day (<0.1 mm d^{-1}) frequency change per degree (% $°C^{-1}$) from (a, b) (SP)CCSM4, (c, d) (SP)CESM1-CAM4, and (e, f) (SP)CESM1-CAM5 for (a, c, e) CAM and (b, d, f) SPCAM simulations; stippling shows significance at 95% confidence based on interannual variability; (SP)CCSM4 is shown at 1° resolution, and (SP)CESM1-CAM4 and (SP)CESM1-CAM5 are shown at 2° resolution.

that not only will infrequent extreme rainfall become more intense, but frequent rain rates that produce the majority of surface reaching rainfall will also become more intense, which may have important implications for the hydrological cycle and water management. Changes in these moderate rates are discussed in more detail in section 3.6 below.

In summary, the distributions reveal several similarities and differences in simulated changes to the character of rainfall in response to climate forcing produced by conventional and superparameterized versions of CAM. Both CAM and SPCAM include a higher frequency and more rain from intense rates in response to future climate forcings relative to their baseline climates. Increasing percentage changes as a function of percentile are also seen in both models, but are more convergent across versions/resolutions in SPCAM. SPCAM has a significant shift in response to climate change smoothly across the amount distribution, including both the moderate amount mode peak and extreme rates, while CAM tends to broaden the distribution without significantly shifting the peak. These differences between the models are dominated by the tropical response; at high latitudes, the two models are almost identical. Additionally, all versions of SPCAM and the latest version of CAM (CESM1-CAM5) show an enhancement of the oceanic drizzle mode. To further investigate the physical mechanisms leading to these changes, sections 3.3–3.6 evaluate the geographic

Table 3. Annual Dry Day Frequency Percent Change With 95% Confidence Interval (% °C^{-1})[a]

Region	CCSM4	SPCCSM4	CESM1-CAM4	SPCESM1-CAM4	CESM1-CAM5	SPCESM1-CAM5
90°S–90°N	0.19 ± 0.18	−0.09 ± 0.63	0.19 ± 0.31	0.14 ± 0.24	0.20 ± 0.15	1.80 ± 0.17
^{L}90°S–90°N	0.04 ± 0.22	1.33 ± 0.27	−0.06 ± 0.36	1.15 ± 0.24	−0.01 ± 0.19	1.20 ± 0.14
^{O}90°S–90°N	0.32 ± 0.29	−2.24 ± 1.11	0.43 ± 0.31	−1.81 ± 0.55	0.54 ± 0.30	2.67 ± 0.40
50°S–50°N	0.82 ± 0.18	0.59 ± 0.78	0.94 ± 0.40	0.90 ± 0.51	1.33 ± 0.36	2.93 ± 0.44
^{L}50°S–50°N	1.05 ± 0.33	2.35 ± 0.41	0.95 ± 0.64	1.94 ± 0.50	0.93 ± 0.48	2.07 ± 0.37
^{O}50°S–50°N	0.68 ± 0.25	−1.72 ± 1.22	0.93 ± 0.26	−0.95 ± 0.84	1.89 ± 0.50	4.04 ± 0.67
90°S–50°S	−2.41 ± 0.33	−2.77 ± 0.66	−2.44 ± 0.33	−2.99 ± 0.33	−2.75 ± 0.31	−2.02 ± 0.27
50°S–15°S	0.64 ± 0.39	−1.16 ± 0.99	1.05 ± 0.66	−0.57 ± 0.74	−1.67 ± 0.84	1.23 ± 0.67
15°S–15°N	1.00 ± 0.39	1.51 ± 1.37	0.38 ± 0.33	1.77 ± 1.14	2.79 ± 1.03	5.32 ± 0.48
15°N–50°N	0.87 ± 0.31	1.19 ± 0.57	1.13 ± 0.44	1.28 ± 0.58	2.31 ± 0.62	2.62 ± 0.37
50°N–90°N	−2.65 ± 0.73	−1.92 ± 0.34	−2.69 ± 0.43	−1.36 ± 0.63	−2.21 ± 0.74	−0.99 ± 0.87

[a]Superscripts L and O denote land-only and ocean-only averaging regions, respectively.

patterns of mean rainfall, dry day frequency, extreme rainfall intensity, and the rainfall amount mode/median change.

3.3. Mean Rainfall Changes

All of the models increase global mean precipitation in a range between 1.3 and 1.7% °C^{-1} (see Table 2). The global mean changes are smallest in both conventional and superparameterized versions of (SP)CESM1-CAM5. The mean changes in SPCAM are also slightly less than CAM in all versions, which result in part from larger reductions in accumulated rainfall from light rates. However, the decrease in light rain and increase in heavy rain do not necessarily occur in the same location, and regional analysis indicates that there are areas with compensating increases and decreases in rainfall. These mean rainfall changes are shown geographically in Figure 6 and over large regional subdomains in Table 2.

Generally, all models increase mean rainfall across the Inter-Tropical Convergence Zone (ITCZ) and at high latitudes (i.e., Southern Ocean), and decrease mean rainfall over subtropical oceans (Figure 6). In CAM, the ITCZ increase enhances the double-ITCZ structure across the central and east equatorial Pacific Ocean. In SPCAM, the ITCZ increase extends further west across the equatorial Pacific Ocean, and concentrates the Northern Hemisphere convergence zone with a southward shift. Interestingly, mean rain in the waters around the Maritime Continent, which has a significant amount of rain in the baseline climate [*Kooperman et al*., 2016, Figure 5], does not increase as much as the East Pacific Ocean in both CAM and SPCAM. This implies a potential for greater mean rainfall sensitivity over colder waters to the east. Moving poleward, all models also show an off-equatorial reduction in rainfall over the Pacific Ocean outside of the ITCZ region, little statistically significant change through the subtropics and midlatitudes, and significant increases over the Southern Ocean and Arctic.

Over land, the mean rainfall response is more complicated and CAM and SPCAM show different regional changes. Overall, mean rainfall on land increases significantly more in CAM than SPCAM, especially between 50°S and 50°N, which shows an annual mean reduction in two versions of SPCAM, while all versions of CAM

Table 4. Annual 99th Percentile Precipitation Rate Percent Change With 95% Confidence Interval (% °C^{-1})[a]

Region	CCSM4	SPCCSM4	CESM1-CAM4	SPCESM1-CAM4	CESM1-CAM5	SPCESM1-CAM5
90°S–90°N	4.05 ± 0.52	3.85 ± 0.43	3.55 ± 0.65	3.73 ± 0.79	3.52 ± 0.68	4.64 ± 0.85
^{L}90°S–90°N	4.60 ± 0.39	4.00 ± 0.39	4.08 ± 1.19	4.80 ± 1.35	3.66 ± 0.60	3.39 ± 0.34
^{O}90°S–90°N	3.88 ± 0.60	3.81 ± 0.50	3.38 ± 0.65	3.43 ± 0.88	3.48 ± 0.77	5.02 ± 1.05
50°S–50°N	3.79 ± 0.58	3.58 ± 0.46	3.17 ± 0.71	3.43 ± 0.83	3.07 ± 0.81	4.43 ± 1.00
^{L}50°S–50°N	4.45 ± 0.51	3.70 ± 0.51	3.67 ± 1.49	4.52 ± 1.60	3.16 ± 0.87	2.91 ± 0.45
^{O}50°S–50°N	3.60 ± 0.64	3.55 ± 0.53	3.03 ± 0.70	3.16 ± 0.94	3.05 ± 0.89	4.86 ± 1.22
90°S–50°S	6.67 ± 0.52	7.55 ± 0.41	7.11 ± 0.80	7.14 ± 0.56	8.43 ± 0.22	8.98 ± 0.78
50°S–15°S	2.66 ± 0.41	3.26 ± 0.64	2.57 ± 0.47	1.95 ± 0.79	3.79 ± 1.13	4.85 ± 1.01
15°S–15°N	4.93 ± 1.49	4.87 ± 0.69	3.88 ± 1.51	5.36 ± 1.34	3.22 ± 1.24	5.98 ± 1.30
15°N–50°N	3.21 ± 0.57	1.62 ± 0.85	2.76 ± 0.83	1.41 ± 1.42	2.13 ± 1.54	1.05 ± 1.45
50°N–90°N	5.18 ± 0.54	4.85 ± 0.32	4.83 ± 0.25	5.29 ± 0.41	3.88 ± 0.40	3.58 ± 0.90

[a]Superscripts L and O denote land-only and ocean-only averaging regions, respectively.

Table 5. Annual Precipitation Amount Mode Percent Change With 95% Confidence Interval (% $°C^{-1}$)[a]

Region	CCSM4	SPCCSM4	CESM1-CAM4	SPCESM1-CAM4	CESM1-CAM5	SPCESM1-CAM5
90°S–90°N	2.91 ± 1.10	5.51 ± 2.14	0.00 ± 1.10	6.17 ± 2.92	1.78 ± 1.64	2.03 ± 5.80
^{L}90°S–90°N	2.91 ± 0.88	5.51 ± 1.69	1.97 ± 1.48	8.65 ± 2.48	1.78 ± 1.33	2.03 ± 4.20
^{O}90°S–90°N	0.00 ± 1.28	5.51 ± 2.23	0.00 ± 0.00	8.65 ± 4.67	1.78 ± 1.21	2.03 ± 3.59
50°S–50°N	0.00 ± 1.08	5.51 ± 1.17	1.97 ± 2.14	8.65 ± 2.69	1.78 ± 0.00	6.71 ± 2.66
^{L}50°S–50°N	2.91 ± 0.66	5.51 ± 1.17	4.15 ± 1.21	8.65 ± 5.96	1.78 ± 1.95	4.25 ± 4.19
^{O}50°S–50°N	0.00 ± 1.51	5.51 ± 2.25	0.00 ± 1.34	6.17 ± 2.08	1.78 ± 0.00	6.71 ± 3.14
90°S–50°S	6.11 ± 1.55	8.68 ± 1.59	6.54 ± 2.20	8.65 ± 2.48	5.88 ± 1.61	9.40 ± 2.96
50°S–15°S	2.91 ± 1.41	5.51 ± 2.63	4.15 ± 2.00	3.91 ± 4.53	3.73 ± 1.33	4.25 ± 1.24
15°S–15°N	0.00 ± 1.12	8.68 ± 1.17	0.00 ± 1.34	8.65 ± 3.79	1.78 ± 0.99	9.40 ± 2.02
15°N–50°N	2.91 ± 2.79	5.51 ± 2.05	6.54 ± 4.50	1.86 ± 3.11	3.73 ± 2.77	4.25 ± 5.35
50°N–90°N	0.00 ± 1.23	2.62 ± 1.70	1.97 ± 4.09	6.17 ± 2.08	1.78 ± 3.71	6.71 ± 2.66

[a]Superscripts L and O denote land-only and ocean-only averaging regions, respectively. Note that the mode is calculated from discrete area-averaged distributions for each region rather than at the grid point level.

have larger percentage increases than the combined land and ocean region (1.72, 1.90, and 0.92% $°C^{-1}$ for CAM and −0.21, 0.59, and −0.88% $°C^{-1}$ for SPCAM from versions (SP)CCSM4, (SP)CESM1-CAM4, and (SP)CESM1-CAM5, respectively; Table 2). All three versions of CAM have significant increases in mean rainfall over central Africa and Australia not seen in any version of SPCAM, and SPCAM has larger reductions in rainfall over South and central America. Over the southwest U.S., the intensity, geographic extent, and statistical significance of future drying are more pronounced in SPCAM than in CAM.

Some of these regional mean rainfall changes may manifest from a change in the frequency of rain and others from a change in the intensity of rain. For example, mean rainfall increases in the ITCZ are associated with a colocated intensification of moderate (Figure 9) rates in SPCAM, which implies an intensity shift across the distribution. However, in CAM, increases in ITCZ mean rainfall are associated with a much smaller moderate rainfall change (Figure 9), implying that mean changes result more from increases in frequency than intensity. Likewise, there are intensity changes that do not register as mean changes due to compensating reductions in light rates and increases in heavy rates in some regions (e.g., Indian Ocean in SPCAM).

3.4. Dry Day Frequency Changes

Decreases in dry day frequency (i.e., more days with rainfall greater than 0.1 mm d^{-1}), greater than −4% $°C^{-1}$, are most pronounced at high latitudes in all models (Figure 7), where surface temperature increases are large (Figure 2). Reductions in sea-ice coverage (not shown), especially over the Arctic Ocean, likely contribute to the high-latitude dry day frequency decrease as well, as more frequent rainfall is driven by larger local surface moisture fluxes over open ocean [*Bintanja and Selten*, 2014]. Broadly over the two high-latitude averaging regions (90°S–50°S and 50°N–90°N), all models have large reductions in dry day frequency between −1.0 and −3.0% $°C^{-1}$ (see Table 3). In combination with increases in rainfall intensity, frequency changes contribute to the significant percentage increases in mean rainfall for these regions as discussed above. Consistency across CAM and SPCAM version pairs adds confidence to this result, and suggests that it is a resilient response of the climate system to anthropogenic forcing.

Generally, all models tend to show an increase in dry day frequency over most land regions, though there are differences on regional scales (e.g., a decrease over Australia in CCSM4 and CESM1-CAM4), and SPCAM's changes tend to be larger than CAM's (1.9–2.4% $°C^{-1}$ for SPCAM versus 0.9–1.1% $°C^{-1}$ for CAM in the region between 50°S and 50°N). The most robust increases in dry day frequency seen across all models occur in Western Europe and Southern Africa. In addition, SPCAM shows significantly larger increases than CAM for the Amazon, central and North America, and the Maritime Continent, especially in versions SPCCSM4 and SPCESM1-CAM4. The increase in days with rain less than 0.1 mm d^{-1} result mostly from decreases in the frequency of days with rates between 1 and 10 mm d^{-1} as shown in Figures 4a–4c. In many regions over land, increased dry day frequency is not always associated with a reduction in mean rainfall because intensity increases compensate, producing the same amount or even more rainfall from less frequent events. For instance, all models show an increase in mean rainfall over Indonesia despite increased dry day frequency.

Dry day frequency changes over the midlatitude and tropical oceans tend to be smaller than over land, since the ocean is not moisture limited and does not depend on the complex coupling mechanisms

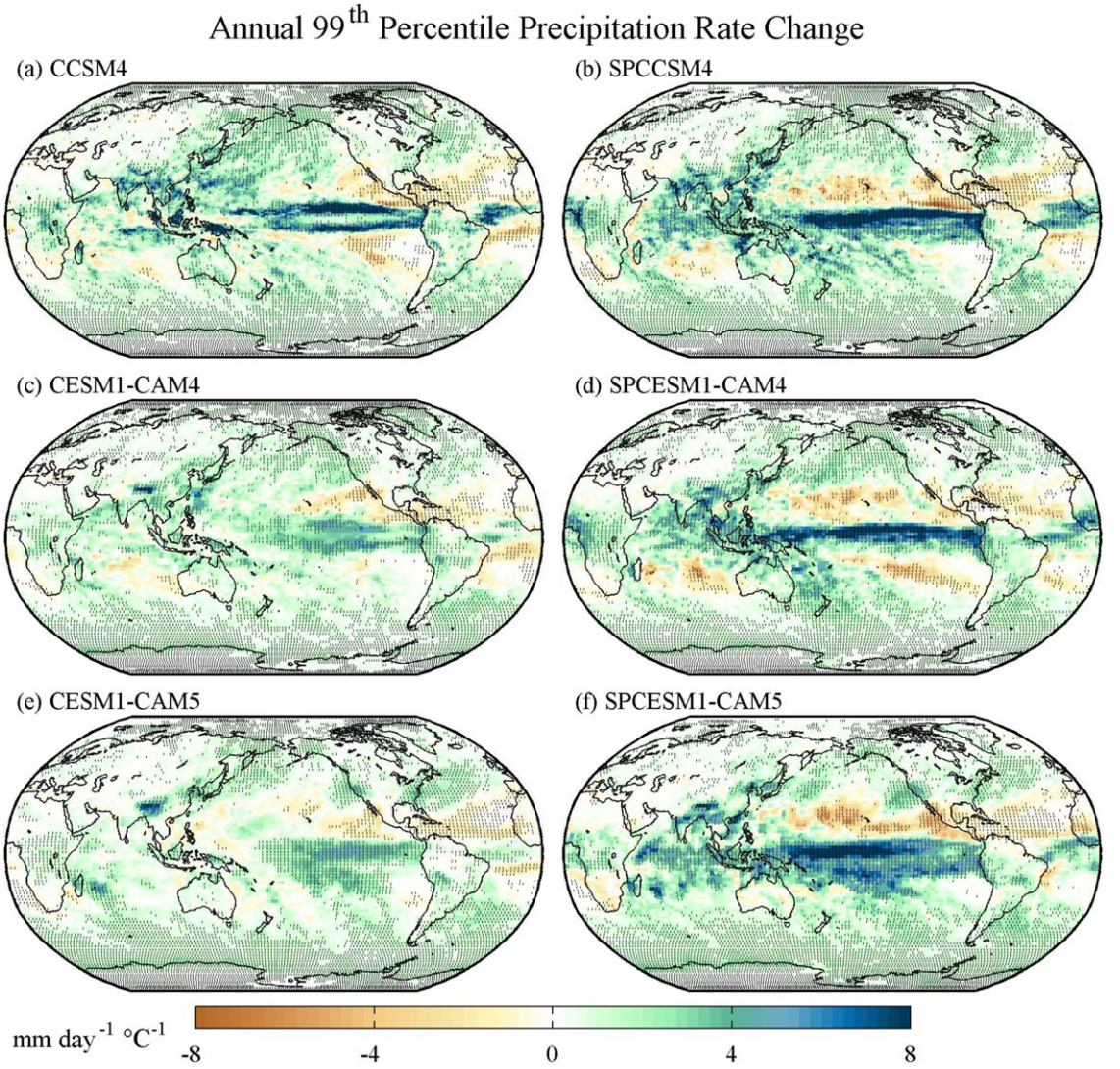

Figure 8. Annual 99th percentile rate change per degree (mm d^{-1} $°C^{-1}$) from (a, b) (SP)CCSM4, (c, d) (SP)CESM1-CAM4, and (e, f) (SP)CESM1-CAM5 for (a, c, e) CAM and (b, d, f) SPCAM simulations; stippling shows significance at 95% confidence based on interannual variability; (SP)CCSM4 is shown at 1° resolution, and (SP)CESM1-CAM4 and (SP)CESM1-CAM5 are shown at 2° resolution.

involving the land-surface (e.g., soil moisture and stomatal conductance). However, the sign of changes in dry day frequency over the ocean appear to be more sensitive to an explicit representation of convection than changes over land (Table 3 land-only versus ocean-only between 50°S and 50°N). In general, the SPCAM versions based on SPCAM4 show a broad reduction in dry day frequency over all oceans (Figures 7b and 7d), especially in subtropical stratocumulus zones, while the counterpart versions of CAM show a decrease along the equatorial central Pacific Ocean, but otherwise a general increase. As mentioned in section 3.2, decreases in dry day frequency in SPCAM are a related to an enhancement of the oceanic drizzle mode (Figures 3a and 3b), which has the largest change off the west coast of most subtropical continents in stratocumulus regions (e.g., California, Peru, and Namibia in Figures 7b and 7d). Comparing Figures 6 and 7, it is clear that frequency changes are not directly relatable to mean rainfall changes because of compensating changes in rainfall intensity. For instance, in the central tropical Pacific Ocean, SPCAM shows very little change in frequency despite a large change in mean rainfall, suggesting most of the mean change is produced by an increase in intensity. However, in CAM, a decrease in the dry day frequency over the tropical central Pacific Ocean in versions CCSM4 and CESM1-CAM4 contributes in part to the increased mean rainfall seen there. Finally, the changes in dry day frequency for the (SP)CESM-CAM5 version of the models (Figures 7e and 7f) are more internally consistent between CAM and SPCAM version pairs, and less

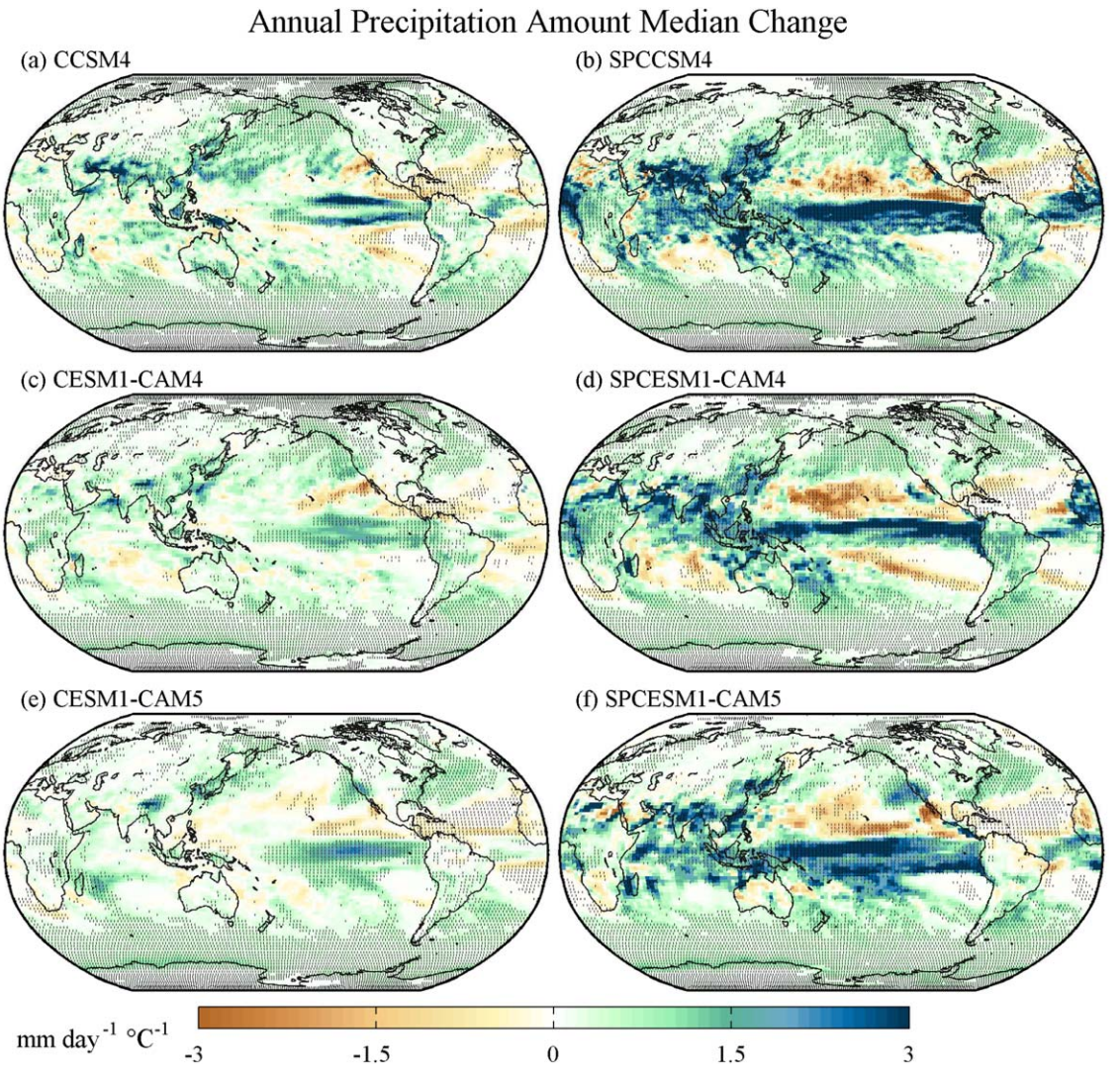

Figure 9. Annual amount median change per degree (mm d^{-1} $°C^{-1}$) from (a, b) (SP)CCSM4, (c, d) (SP)CESM1-CAM4, and (e, f) (SP)CESM1-CAM5 for (a, c, e) CAM and (b, d, f) SPCAM simulations; stippling shows significance at 95% confidence based on interannual variability; (SP)CCSM4 is shown at 1° resolution, and (SP)CESM1-CAM4 and (SP)CESM1-CAM5 are shown at 2° resolution.

consistent with the earlier model versions. In the (SP)CESM-CAM5 results, there are large increases in dry day frequency off the west coast of Africa and central and South America, which may be related to new or updated physics (e.g., aerosol, cloud microphysics, and land surface) not represented in earlier versions of the models.

3.5. Extreme Rainfall Intensity Changes

There are many ways to evaluate changes in extreme rainfall intensity including percentage changes (i.e., % $°C^{-1}$, as shown in Figures 3 and 4) and absolute changes (i.e., mm d^{-1} $°C^{-1}$) as a function of percentile, or changes in the amount of rain from rates above a threshold. In *Kooperman et al*. [2016], we evaluated the geographic pattern of both 99th percentile rates and accumulated rain from rates above a threshold of 50 mm d^{-1}. Since conventional versions of CAM produce very little rain above this threshold value, it does not provide a useful comparison between the two model versions, so here we focus on percentile changes instead. As stated earlier, percentile percentage changes can draw a useful connection to theoretical constraints, but are less relevant for physical processes and potentially mask present-day biases. Therefore, as a complement to the percentile percentage changes shown in Figures 3 and 4, Figure 8 depicts absolute changes (mm d^{-1} $°C^{-1}$) in the 99th percentile precipitation rates including all dry and rainy days.

With the exception of the North Pacific and North Atlantic subtropical oceans, all models generally increase the intensity of 99th percentile rainfall in response to climate forcing. The largest increases are seen across the ITCZ, which is more than 8 mm d^{-1} $°C^{-1}$ in all versions of SPCAM and in the highest-resolution (1°) version of CAM (i.e., CCSM4). Globally, in terms of percentage changes, this represents an increase between 3.5 and 4.6% $°C^{-1}$ in all models (Table 4 and Figures 3g–3i). Although the absolute changes are smaller in CESM1-CAM4 and CESM1-CAM5 relative to other models, the baseline present-day/preindustrial rates were also lower than CCSM4 and SPCAM [*Kooperman et al*., 2016], such that small absolute changes produce similar percentage changes. The general pattern of change is also similar in 2° and 1° versions of CAM.

However, honing in on the tropics alone (15°S–15°N in Table 4), the lower resolution versions of CAM (2°) do not capture the percentage or absolute change simulated by their SPCAM counterparts (i.e., 3.2–3.9% $°C^{-1}$ in CAM versus 5.4–6.0% $°C^{-1}$ in SPCAM). Global agreement is largely due to the similarity of percentage responses outside of the tropics in the two model versions (see Table 4). In the tropics, the missing physics of organized convection that likely leads to weak present-day rates also leads to a weak climate change response in CAM. In the 1° version of CCSM4, more of the extreme response is controlled by resolved-scale processes, producing a response that is surprisingly consistent with SPCCSM4 results across all latitude bands, including the tropics (i.e., 4.9% $°C^{-1}$ in both model versions), indicating a scale dependence of precipitation extremes in the conventionally parameterized version of CAM. This scale dependence is reassuringly absent in SPCAM, which produces a fairly resilient tropical response and pattern across all versions and both 1° and 2° resolutions.

Evaluating the spatial pattern of extreme rain rate changes across the tropics reveals some important differences between CAM and SPCAM. In general, CAM tends to increase the intensity within its double ITCZ rain bands in the central and eastern Pacific Ocean. In SPCAM, the Northern Hemisphere ITCZ-band intensification expands across the Pacific Ocean, consistent with the mean rainfall increase. However, SPCAM also exhibits telling regional geographic action centers of extreme rain increases along the equatorial tropical West Pacific, throughout the Indian Ocean, and across the Maritime Continent and its surrounding waters. These action centers are weaker or absent in CAM. There is also a consistent increase in 99th percentile rates around the coast of northwest Africa in SPCAM that is missing in the lower resolution versions of CAM. These geographic patterns of extreme rain response in SPCAM are evocative of the activity centers of the MJO, Indian and Asian monsoons, and African easterly waves. This pattern is also consistent with regions that have the most intense rates in the present-day/preindustrial climate [*Kooperman et al*., 2016]. Connections to these important tropical modes of variability are discussed in terms of changes to the entire distribution, as measured by responses that include both moderate and extreme rates, in section 3.6 below.

3.6. Rainfall Amount Mode/Median Changes

While the effects of superparameterization on extreme rain rates in the tropics are already striking, focusing on moderate rain rates turns out to be especially revealing.

Figure 9 shows that, similar to the extreme precipitation response, all models tend to increase the intensity of moderate rainfall everywhere except subtropical ocean regions, as demonstrated by the spatial patterns of median precipitation rate changes (Figure 9) and precipitation amount mode changes (supporting information Figure S1 and Table 5). As mentioned for Figure 5 earlier, changes in the peak of the amount distribution (i.e., the "amount mode") are similar at high latitudes in the two models, especially for the Southern Hemisphere between 90°S and 50°S where all models show a percentage change between 5.9 and 9.4% $°C^{-1}$ (see Table 5).

However, equatorward of 50° the models begin to diverge, showing a large shift between 5.5 and 8.7% $°C^{-1}$ in SPCAM and a small shift between 0.0 and 2.0% $°C^{-1}$ in CAM. Focusing on the tropics between 15°S and 15°N, this difference is even larger, between 6.7 and 9.4% $°C^{-1}$ in SPCAM and 0.0 and 1.8% $°C^{-1}$ in CAM. Much smaller percentage changes are simulated in CAM despite the fact that present-day/preindustrial rates were already weaker than observed and simulated by SPCAM [*Kooperman et al*., 2016]. Unlike the extreme precipitation response, the higher-resolution version of CAM does not capture the magnitude of increase in the amount mode that is simulated by SPCAM. This may be due to the fact that the amount mode is controlled by parameterized convective rainfall in CAM, which generates the majority of rain in the tropics, while resolved large-scale rain, which increases with higher resolution, contributes more to the extreme rates (not shown).

Absolute changes (mm d^{-1} $°C^{-1}$) in the geographic pattern of median rain rates shown in Figure 9 depict differences in the rainfall response between CAM and SPCAM that are even more visually revealing than the percentage changes discussed for Table 5 above. From Figure 9 it is clear the conventional versions of CAM are unable to capture the moderate rain rate intensity shifts simulated across the tropics by all versions of SPCAM. In SPCAM, moderate rainfall increases across the ITCZ in a similar pattern as the mean (Figure 6) and extreme (Figure 8) rain rates. However, for the amount median, the geographic pattern is more widespread than the mean, including many densely populated regions. Intensification across the MJO and monsoon regional activity centers (i.e., Indian Ocean, Asia, Maritime Continent, and northwest Africa) is much more striking for moderate rates than it was for the mean or extremes. This suggests a significant shift in the intensity of most rainfall for these regions that is modulated by the intensification of organized convection, which does not project significantly onto mean rainfall (Figure 6) due to associated reductions in rainfall frequency (Figure 7).

In this section, we have focused on geographic changes in median rates (Figure 9) because the amount mode can be difficult to calculate at the grid point level for reasons discussed earlier. However, changes in the amount mode are included in supporting information Figure S2, which are noisy but show similar patterns as the median, except in regions of very little rainfall where distributions are under sampled, such as the subtropical southeast Pacific Ocean near the coast South America in SPCCSM4 (plot b). For large zonal average regions, the amount mode can be fit more reliably, and is therefore the quantity given in Table 5. Though the median and amount mode are not the same metric, they both describe changes to moderate rates that generate the majority of surface reaching rainfall, and highlight similar rainfall patterns in present-day/preindustrial [*Kooperman et al*., 2016] and future climate simulations.

In this study, we have chosen to limit our analysis to the annual mean changes in rainfall intensity revealed by 99th percentile and median/mode rates discussed above. However, these results suggest an important role of the MJO and monsoons in driving submonthly rainfall intensity changes; and previous work has shown that the MJO becomes stronger, faster, and bigger with climate change [*Arnold et al*., 2014; *Pritchard and Yang*, 2016]. While it is outside the scope of the current work to include detailed analysis of seasonal and intraseasonal time scales, offline analysis (not shown) conditioning the daily rainfall variance on MJO-amplitude, suggests an important part of the intensification of moderate rainfall (shown in Figure 9) is associated with high MJO-amplitude days. Similarly, future changes in monsoon rainfall simulated by SPCAM increase the intensity of rain rates most during peak monsoon months.

4. Summary and Conclusions

In this study, we have analyzed the response of daily rainfall to climate forcing as simulated by conventional and superparameterized versions of the Community Atmosphere Model, focusing on statistics of rainfall frequency and amount distributions including mean, dry day frequency, and moderate and extreme rates. Robust effects of explicitly resolved convection represented by superparameterization were assessed by identifying rainfall changes that manifest across three different versions of SPCAM relative to their CAM counterparts. We have focused on signatures of climate change that are consistent across multiple forcing scenarios, changes between the beginning and end of the 21st century under RCP8.5 conditions in (SP)CCSM4 and changes between preindustrial and $4 \times CO_2$ concentrations in (SP)CESM1-CAM4 and (SP)CESM1-CAM5. Although these scenarios produce different global mean temperature changes (3.4–3.8°C for RCP8.5 versus 4.9–5.6°C for 4X CO_2), the signatures are robust; normalization by global mean temperature change reveals important differences in the rainfall response simulated by the two model classes, and sensitivity to version/resolution, particularly in the tropics.

Time mean and global mean rainfall changes are broadly similar in SPCAM and CAM, with geographic patterns dominated by a classic ITCZ-amplification, ITCZ-focusing, or ITCZ-shift response. Regionally, SPCAM has a larger rainfall increase in the tropical Pacific, and a smaller increase or even decrease in the subtropics/midlatitudes. Both models increase the amount of rain contributed by heavier rates, but SPCAM has a bigger reduction in the amount of rain from rates less than 20 mm d^{-1}, especially over land and in the tropics. The *dry day frequency* increases over land, particularly in SPCAM due to a decrease in light rain events. Over the ocean, there is a significant enhancement of the oceanic drizzle mode peak in the earlier versions of SPCAM and to some extent both the conventional and superparameterized versions of (SP)CESM1-CAM5. The relationship between these dry day frequency and mean rainfall changes has implications for changes in rain rate intensity. For example, the mean ITCZ increase in CCSM4 and CESM1-CAM4

is accompanied by a decrease in dry day frequency, which is not seen in any version of SPCAM, implying that mean ITCZ increases in SPCAM are driven instead by increases in intensity.

Extreme rainfall intensity changes reveal a distribution shift toward heavier rates that is much greater in all versions of SPCAM than in CAM. Percentile percentage changes appear to converge to values between 5 and 7% $°C^{-1}$ in all versions of SPCAM, independent of resolution, but continue to increase with higher percentiles in CAM and exhibit sensitivity to 1° versus 2° horizontal resolution. Over land, all versions of SPCAM reach a maximum increase of 7% $°C^{-1}$. In contrast, the highest-resolution version of CAM (i.e., CCSM4) reaches nearly 11% $°C^{-1}$ relative to 7% $°C^{-1}$ in the lower resolution versions. When evaluated geographically in terms of absolute changes (mm d^{-1} $°C^{-1}$), 99th percentile rates increase significantly more in SPCAM than CAM, most notably in the tropics across the ITCZ and over the Indian and West Pacific Oceans. The scale-insensitive behavior to changes in GCM-resolution exhibited by SPCAM demonstrates its potential for even higher global and variable resolution simulations. Ongoing development of the approach in a quasi-3D (Q3D) framework may even soon provide a fully scale-aware global model [*Jung and Arakawa*, 2014].

Rainfall amount mode/median changes are radically different in SPCAM and CAM in the tropics (Figure 9). SPCAM shows a significant intensification of moderate rain rates in key tropical activity centers, while CAM shows very little change in all model versions. Changes in the amount mode are not commonly analyzed in climate models. We have investigated them as changes in the peak of the amount distributions (i.e., Figures 3d–3f, 4d–4f, and 5), over large zonal averages regions (i.e., Table 5), and geographically as changes in the amount median (Figure 9).

Even the higher-resolution version of CAM is not able to capture the changes in moderate rainfall intensity simulated by SPCAM, which shows a significant intensification of the rain rates that deliver most accumulated rainfall across the ITCZ, MJO, and monsoon regions. These regions suggest that organized convection modulated by tropical wave modes is an especially important driver of the overall intensity of most rainfall events, in addition to extreme values. Conventionally parameterized models that do not explicitly simulate certain tropical wave modes, such as the MJO, and that do not sufficiently modulate submonthly rainfall by the monsoon, may not be able to capture these important changes. That is, CAM exhibits a stubbornly stationary amount mode across climates. The response to climate change of moderate rates that generate the majority of surface reaching rainfall are a key characteristic of the hydrological cycle that influences canopy water collection, ground water infiltration, and surface runoff. This may have important implications for drought and flood prediction, as well ground water storage and the availability of freshwater for natural ecosystems and human use.

Overall, these results highlight an important difference in the rainfall response to climate change when convection is resolved rather than parameterized within the NCAR Community Atmosphere Model—SPCAM shows a smooth shift of the entire distribution to heavier rain rates, while CAM has a broadening response, separately increasing the amount of rain from moderate and extreme rates. SPCAM suggests that not only will the infrequent extreme events become more intense, but frequent moderate events that generate the majority of accumulated rain will also become more intense. This result has vital implications for human impacts—preparing for future changes in water resource management and hazardous events should consider changes in the full character of rainfall, not just the most extreme features.

Acknowledgments

Kooperman acknowledges funding for this work from an NSF Postdoctoral Research Fellowship (AGS-1349579). Pritchard acknowledges funding from the NSF (AGS-1419518) and DOE (DE-SC0012152 and DE-SC0012548). CESM development is led by NCAR and supported by the NSF and DOE; NCAR is sponsored by the NSF. Development of superparameterization is led by CMMAP (www.cmmap.org), funded by the NSF (ATM-0425247) and managed by Colorado State University. CESM (release code repository) and SPCESM (development code repository) are available for public download through the NCAR subversion code repository (https://www2.cesm.ucar.edu). CCSM4 simulations were run at the DOE National Center for Computational Sciences at Oak Ridge National Laboratory (DE-AC05-00OR22725). SPCCSM4 simulations were run at the DOE National Energy Research Scientific Computing Center (DE-AC02-05CH11231) and supported by the Regional and Global Climate Modeling Program (SC0006722). (SP)CESM1-CAM4 and (SP)CESM1-CAM5 simulations were run at the NSF NCAR Computational and Information Systems Laboratory on Yellowstone (UCIR0012 and UCSU0006). SPCCSM4 and CCSM4 output is available on the Earth System Grid (www.earthsystemgrid.org). (SP)CESM1-CAM4 and (SP)CESM1-CAM5 output is available on request from mark@atmos.colostate.edu and mburt@atmos.colostate.edu, respectively. The authors are grateful to Cristiana Stan and Li Xu for providing SPCCSM4 output. The authors also thank A. Pendergrass, an anonymous reviewer, and the Editor for many comments that improved this article.

References

Allan, R. P., and B. J. Soden (2008), Atmospheric warming and the amplification of precipitation extremes, *Science*, *321*, 1481–1484.

Allen, M. R., and W. J. Ingram (2002), Constraints on future changes in climate and the hydrologic cycle, *Nature*, *419*, 224–232.

Arakawa, A., and W. H. Schubert (1974), Interaction of a cumulus cloud ensemble with the large-scale environment, Part I, *J. Atmos. Sci.*, *31*, 674–701.

Arnold, N. P., M. Branson, M. A. Burt, D. S. Abbot, Z. Kuang, D. A. Randall, and E. Tziperman (2014), Effects of explicit atmospheric convection at high CO_2, *Proc. Natl. Acad. Sci. U. S. A.*, *111*, 10,943–10,948.

Benedict, J. J., and D. A. Randall (2009), Structure of the Madden-Julian oscillation in the superparameterized CAM, *J. Atmos. Sci.*, *66*(11), 3277–3296.

Berg, P., C. Moseley, and J. O. Haerter (2013), Strong increase in convective precipitation in response to higher temperatures, *Nat. Geosci.*, *6*, 181–185.

Bintanja, R., and F. M. Selten (2014), Future increases in Arctic precipitation linked to local evaporation and sea ice retreat, *Nature*, *509*, 479–482.

Bretherton, C. S., and S. Park (2009), A new moist turbulence parameterization in the Community Atmosphere Model, *J. Clim.*, *22*, 3422–3448.

Chou, C., C.-A. Chen, P.-H. Tan, and K. T. Chen (2012), Mechanisms for global warming impacts on precipitation frequency and intensity, *J. Clim.*, *25*(9), 3291–3306.

DeMott, C. A., D. A. Randall, and M. Khairoutdinov (2007), Convective precipitation variability as a tool for general circulation model analysis, *J. Clim.*, *20*, 91–112.
DeMott, C. A., C. Stan, D. A. Randall, J. L. Kinter III, and M. Khairoutdinov (2011), The Asian monsoon in the superparameterized CCSM and its relationship to tropical wave activity, *J. Clim.*, *24*, 5134–5156.
Gent, P. R., et al. (2011), The Community Climate System Model Version 4, *J. Clim.*, *24*, 4973–4991.
Gustafson, W. I., Jr., L. K. Berg, R. C. Easter, and S. J. Ghan (2008), The Explicit-Cloud Parameterized-Pollutant hybrid approach for aerosol-cloud interactions in multiscale modeling framework models: Tracer transport results, *Environ. Res. Lett.*, *3*, 025005.
Gustafson, W. I., Jr., P.-L. Ma, and B. Singh (2014), Precipitation characteristics of CAM5 physics at mesoscale resolution during MC3E and the impact of convective timescale choice, *J. Adv. Model. Earth Syst.*, *6*, 1271–1287, doi:10.1002/2014MS000334.
Hack, J. J. (1994), Parameterization of moist convection in the National Center for Atmospheric Research Community Climate Model (CCM2), *J. Geophys. Res.*, *99*, 5551–5568.
Hunke, E. C., and W. H. Lipscomb (2008), CICE: The Los Alamos sea ice model user's manual, version 4, *Tech. Rep. LA-CC-06-012*, 76 pp., Los Alamos Natl. Lab., Los Alamos, N. M.
Iacono, M. J., J. S. Delamere, E. J. Mlawer, M. W. Shephard, S. A. Clough, and W. D. Collins (2008), Radiative forcing by long-lived greenhouse gases: Calculations with the AER radiative transfer models, *J. Geophys. Res.*, *113*, D13103, doi:10.1029/2008JD009944.
Jung, J.-H., and A. Arakawa (2014), Modeling the moist-convective atmosphere with a Quasi-3-D Multiscale Modeling Framework (Q3D MMF), *J. Adv. Model. Earth Syst.*, *6*, 1–21, doi:10.1002/2013MS000295.
Khairoutdinov, M., D. Randall, and C. DeMott (2005), Simulations of the atmospheric general circulation using a cloud-resolving model as a superparameterization of physical processes, *J. Atmos. Sci.*, *62*(7), 2136–2154.
Khairoutdinov, M. F., and D. A. Randall (2001), A cloud resolving model as a cloud parameterization in the NCAR Community Climate System Model: Preliminary results, *Geophys. Res. Lett.*, *28*, 3617–3620.
Kooperman, G. J., M. S. Pritchard, and R. C. J. Somerville (2013), Robustness and sensitivities of Central U.S. summer convection in the superparameterized CAM: Multi-model intercomparison with a new regional EOF index, *Geophys. Res. Lett.*, *40*, 3287–3291, doi:10.1002/grl.50597.
Kooperman, G. J., M. S. Pritchard, and R. C. J. Somerville (2014), The response of US summer rainfall to quadrupled CO_2 climate change in conventional and super-parameterized versions of the NCAR Community Atmosphere Model, *J. Adv. Model. Earth Syst.*, *6*, 859–882, doi:10.1002/2014MS000306.
Kooperman, G. J., M. S. Pritchard, M. A. Burt, M. D. Branson, and D. A. Randall (2016), Robust effects of cloud superparameterization on simulated daily rainfall intensity statistics across multiple versions of the Community Earth System Model, *J. Adv. Model. Earth Syst.*, *8*, 1–26, doi:10.1002/2015MS000574.
Kopparla, P., E. M. Fischer, C. Hannay, and R. Knutti (2013), Improved simulation of extreme precipitation in a high-resolution atmosphere model, *Geophys. Res. Lett.*, *40*, 5803–5808, doi:10.1002/2013GL057866.
Lawrence, D. M., et al. (2011), Parameterization improvements and functional and structural advances in version 4 of the Community Land Model, *J. Adv. Model. Earth Syst.*, *3*, M03001, doi:10.1029/2011MS00045.
Liu, X., et al. (2012), Toward a minimal representation of aerosols in climate models: Description and evaluation in the Community Atmosphere Model CAM5, *Geosci. Model Dev.*, *5*(3), 709–739.
Li, F., D. Rosa, W. D. Collins, and M. F. Wehner (2012), "Superparameterization": A better way to simulate regional extreme precipitation?, *J. Adv. Model. Earth Syst.*, *4*, M04002, doi:10.1029/2011MS000106.
Martins, G., C. von Randow, G. Sampaio, and A. J. Dolman (2015), Precipitation in the Amazon and its relationship with moisture transport and tropical Pacific and Atlantic SST from the CMIP5 simulation, *Hydrol. Earth Syst. Sci. Discuss.*, *12*, 671–704.
McCrary, R. R., D. A. Randall, and C. Stan (2014), Simulations of the West African Monsoon with a superparameterized climate model. Part II: African easterly waves, *J. Clim.*, *27*, 8323–8341.
Meehl, G. A., et al. (2012), Climate system response to external forcings and climate change projections in CCSM4, *J. Clim.*, *25*, 3661–3683.
Morrison, H., and A. Gettelman (2008), A new two-moment bulk stratiform cloud microphysics scheme in the Community Atmosphere Model, version 3 (CAM3). Part I: Description and numerical tests, *J. Clim.*, *21*(15), 3642–3659.
Morrison, H., J. A. Curry, and V. I. Khvorostyanov (2005), A new double-moment microphysics parameterization for application in cloud and climate models. Part I: Description, *J. Atmos. Sci.*, *62*(6), 1665–1677.
Neale, R. B., et al. (2010a), *NCAR Technical Note: Description of the NCAR Community Atmosphere Model (CAM 4.0)*, Natl. Cent. for Atmos. Res., Boulder, Colo.
Neale, R. B., et al. (2010b), *NCAR Technical Note: Description of the NCAR Community Atmosphere Model (CAM 5.0)*, Natl. Cent. for Atmos. Res., Boulder, Colo
O'Brien, T. A., W. D. Collins, K. Kashinath, O. Rubel, S. Byna, J. Gu, H. Krishnan, and P. A. Ullrich (2016), Resolution dependence of precipitation statistical fidelity in hindcast simulations, *J. Adv. Model. Earth Syst.*, *8*, 976–990.
O'Gorman, P. A. (2012), Sensitivity of tropical precipitation extremes to climate change, *Nat. Geosci.*, *5*, 697–700.
O'Gorman, P. A. (2015), Precipitation extremes under climate change, *Curr. Clim. Change. Rep.*, *1*, 49–59.
O'Gorman, P. A., and T. Schneider (2009), The physical basis for increases in precipitation extremes in simulations of 21st-century climate change, *Proc. Natl. Acad. Sci. U. S. A.*, *106*(35), 14,773–14,777.
Park, S., and C. S. Bretherton (2009), The University of Washington shallow convection and moist turbulence schemes and their impact on climate simulations with the Community Atmosphere Model, *J. Clim.*, *22*(12), 3449–3469.
Pendergrass, A. G., and E. P. Gerber (2016), The rain is askew: Two idealized models relating vertical velocity and precipitation distributions in a warming world, *J. Clim.*, *29*, 6445–6462.
Pendergrass, A. G., and D. L. Hartmann (2014a), The atmospheric energy constraint on global-mean precipitation change, *J. Clim.*, 27, 757–768.
Pendergrass, A. G., and D. L. Hartmann (2014b), Two modes of change of the distribution of rain, *J. Clim.*, *27*, 8357–8371.
Pendergrass, A. G., and D. L. Hartmann (2014c), Changes in the distribution of rain frequency and intensity in response to global warming, *J. Clim.*, *27*, 8372–8383.
Pritchard, M. S., and C. S. Bretherton (2014), Causal evidence that rotational moisture advection is critical to the superparameterized Madden–Julian Oscillation, *J. Atmos. Sci.*, *71*, 800–815.
Pritchard, M. S., and R. C. J. Somerville (2009a), Assessing the diurnal cycle of precipitation in a multi-scale climate model, *J. Adv. Model. Earth Syst.*, *1*, 12, doi:10.3894/JAMES.2009.1.12.
Pritchard, M. S., and R. C. J. Somerville (2009b), Empirical orthogonal function analysis of the diurnal cycle of precipitation in a multi-scale climate model, *Geophys. Res. Lett.*, *36*, L05812, doi:10.1029/2008GL036964.

Pritchard, M. S., and D. Yang (2016), Response of the superparameterized Madden-Julian Oscillation to extreme climate and basic state variation challenges a moisture mode view, *J. Clim.*, *29*, 4995–5008.
Pritchard, M. S., M. W. Moncrieff, and R. C. J. Somerville (2011), Orogenic propagating precipitation systems over the United States in a global climate model with embedded explicit convection, *J. Atmos. Sci.*, *68*(8), 1821–1840.
Randall, D., M. Khairoutdinov, A. Arakawa, and W. Grabowski (2003), Breaking the cloud parameterization deadlock, *Bull. Am. Meteorol. Soc.*, *84*(11), 1547–1564.
Raymond, D. J., and A. M. Blyth (1992), Extension of the stochastic mixing model to cumulonimbus clouds, *J. Atmos. Sci.*, *49*(21), 1968–1983.
Richter, J. H., and P. J. Rasch (2008), Effects of convective momentum transport on the atmospheric circulation in the Community Atmosphere Model, version 3, *J. Clim.*, *21*, 1487–1499.
Rosa, D., and W. D. Collins (2013), A case study of sub-daily simulated and observed continental convective precipitation: CMIP5 and multiscale global climate models comparison, *Geophys. Res. Lett.*, *40*, 5999–6003, doi:10.1002/2013GL057987.
Seneviratne, S. I., T. Corti, E. L. Davin, M. Hirschi, E. B. Jaeger, I. Lehner, B. Orlowsky, and A. J. Teuling (2010), Investigating soil moisture–climate interactions in a changing climate: A review, *Earth Sci. Rev.*, *99*, 125–161.
Smith, R. D., et al. (2010), The Parallel Ocean Program (POP) reference manual, *Tech. Rep. LAUR-10-01853*, 140 pp., Los Alamos Natl. Lab., Los Alamos, N. M.
Stan, C., and L. Xu (2014), Climate simulations and projections with a superparameterized climate model, *Environ. Modell. Software*, *60*, 134–152.
Stephens, G. L., and T. D. Ellis (2008), Controls of global-mean precipitation increases in global warming GCM experiments, *J. Clim.*, *21*, 6141–6155.
Stocker, T. F., D. Qin, G.-K. Plattner, M. Tignor, S. K. Allen, J. Boschung, A. Nauels, Y. Xia, V. Bex, and P. M. Midgley (Eds.) (2013), *Climate Change 2013: The Physical Science Basis. Contribution of Working Group I to the Fifth Assessment Report of the Intergovernmental Panel on Climate Change*, Cambridge Univ. Press, Cambridge, U. K.
Stouffer, R. J., et al. (2006), Investigating the causes of the response of the thermohaline circulation to past and future climate changes, *J. Clim.*, *19*, 1365–1387.
Sun, Y., S. Solomon, A. Dai, and R. W. Portmann (2006), How often does it rain?, *J. Clim.*, *19*, 916–934.
Sun, Y., S. Solomon, A. Dai, and R. W. Portmann (2007), How Often Will It Rain?, *J. Clim.*, *20*, 4801–4818.
Taylor, K. E., R. J. Stouffer, and G. A. Meehl (2012), An overview of CMIP5 and the experiment design, *Bull. Am. Meteorol. Soc.*, *93*, 485–498.
Thibeault, J. M., and A. Seth (2014), A framework for evaluating model credibility for warm-season precipitation in north-eastern North America: A case study of CMIP5 simulations and projections, *J. Clim.*, *27*, 493–510.
Trenberth, K. E. (2011), Changes in precipitation with climate change, *Clim. Res.*, *47*, 123–138.
Wang, M., et al. (2011), The multi-scale aerosol-climate model PNNL-MMF: Model description and evaluation, *Geosci. Model Dev.*, *4*(1), 137–168.
Williamson, D. L. (2013), The effect of time steps and time-scales on parametrization suites, *Q. J. R. Meteorol. Soc.*, *139*, 548–560.
Yang, Q., L. R. Leung, S. A. Rauscher, T. D. Ringler, and M. A. Taylor (2014), Atmospheric moisture budget and spatial resolution dependence of precipitation extremes in aquaplanet simulations, *J. Clim.*, *27*(10), 3565–3581.
Yin, L., R. Fu, E. Shevliakova, and R. E. Dickinson (2013), How well can CMIP5 simulate precipitation and its controlling processes over tropical South America?, *Clim. Dyn.*, *41*(11), 3127–3143.
Zhang, G. J., and N. A. McFarlane (1995), Sensitivity of climate simulations to the parameterization of cumulus convection in the Canadian climate center general-circulation model, *Atmos. Ocean*, *33*(3), 407–446.
Zhu, X., and C. Stan (2015), Projection of summer precipitation over the southeastern United States in the superparameterized CCSM4, *J. Clim.*, *28*, 8052–8066.